# Nogo receptor 1 is a novel class of NK cell inhibitory receptor to destabilize synapse by regulating actin dynamics

**Tae-Don Kim** ( tdkim@kribb.re.kr )
Korea Research Institute of Bioscience and Biotechnology
**Junsang Doh**
Department of Materials Science and Engineering, Seoul National University,
**Se-Chan Oh**
Korea Research Institute of Bioscience and Biotechnology (KRIBB) https://orcid.org/0000-0003-0088-7580
**Seong-Eun Kim**
Pohang University of Science and Technology (POSTECH)
**Seok-Min Kim**
Korea Research Institute of Bioscience and Biotechnology
**Soo Yun Lee**
Korea Research Institute of Bioscience and Biotechnology (KRIBB)
**Sun-Young Lee**
Korea Research Institute of Bioscience and Biotechnology (KRIBB)
**In Hwan Jang**
Korea Research Institute of Bioscience and Biotechnology (KRIBB)
**In-Sun Chu**
Korea Research Institute of Bioscience and Biotechnology (KRIBB)

**Article**

**Keywords:**

**Posted Date:** May 27th, 2022

**DOI:** https://doi.org/10.21203/rs.3.rs-1680869/v1

# Nogo receptor 1 is a novel class of NK cell inhibitory receptor to destabilize synapse by regulating actin dynamics

**Se-Chan Oh[1,2], Seong-Eun Kim[3], Seok-Min Kim[1,2], Soo Yun Lee[1], Sun-Young Lee[1,4], In Hwan Jang[5,6], In-Sun Chu[5,6], Junsang Doh[7]* and Tae-Don Kim[1,2]***

1 Immunotherapy Research Center, Korea Research Institute of Bioscience and Biotechnology (KRIBB), Daejeon, 34141, Republic of Korea
2 Department of Functional Genomics, KRIBB School of Bioscience, Korea University of Science and Technology (UST), Daejeon, 34113, Republic of Korea
3 Department of Mechanical Engineering, Pohang University of Science and Technology (POSTECH), Pohang 37673, Republic of Korea
4 Department of Life Sciences, Korea University, Seoul 02841, Republic of Korea
5 Genome Editing Research Center, Korea Research Institute of Bioscience and Biotechnology (KRIBB), Daejeon, 34141, Republic of Korea
6 Department of Bioinformatics, KRIBB School of Bioscience, Korea University of Science and Technology (UST), Daejeon, 34113, Republic of Korea
7 Department of Materials Science and Engineering, Research Institute of Advanced Materials (RIAM), Institute of Engineering Research, Seoul National University, Seoul 08826, Republic of Korea
* Correspondence: jsdoh@snu.ac.kr and tdkim@kribb.re.kr

## Abstract

The formation of immunological synapse (IS) is essential for natural killer (NK) cells to eliminate target cells. Although elucidation of the overall characteristics and formation processes of IS is ongoing, the mechanisms for regulating the stability of IS by cytoskeleton remain to be understood. The current study reports that Nogo receptor 1 (NgR1) plays a key role in modulating NK cell-mediated killing by destabilization of IS formation. NgR1 deficiency or blockade results in improved tumor control of NK cells by enhancing NK-to-target cell contact stability and regulating F-actin dynamics during IS formation. Clinically, patients with a tumor expressing abundant NgR1 ligand showed poor prognosis despite high levels of NK cell infiltration. Thus, our study identifies NgR1 as an immune checkpoint involved in IS formation and reveals a potential approach to improve the killing effect of NK cells in cancer immunotherapy.

Cancer immunotherapy has been applied, for decades, to eliminate tumors, and various types of immune cells have been used for the purpose, especially those that can lyse target cells via cell-to-cell contact[1, 2]. Natural killer (NK) cells are used in cancer immunotherapy owing to their natural properties, such as the advantages of using allogeneic NK cells for adoptive transfer, safety against cytokine release syndrome, and serving as a first-line defender for target cells[3, 4]. NK cells form an immunological synapse (IS), based on cell-to-cell contact, to recognize and eliminate virus-infected and transformed cancer cells[5, 6, 7, 8, 9, 10, 11]. IS is a dynamic supramolecular structure, where spatiotemporal organization of the cytoskeleton, surface receptors, and intracellular signaling proteins occurs for signal integration and directed secretion of effector molecules[9, 12]. NK cell-IS formation is a multi-step sequential event comprising of initiation of a transient contact for target cell surveillance, establishment of firm adhesion mediated by adhesion molecules and cytoskeleton remodeling, and polarization and excretion of lytic granules for target cell lysis[10, 13, 14, 15]. Activating and inhibitory signals, integrated through the IS, determine target cell fates. Inhibitory signals typically work in the early stages of IS to interfere with activating signals that form and stabilize the IS through cytoskeleton remodeling leading to NK-target interactions, thereby acting as immune checkpoints[11, 16, 17]. Existing immune checkpoint inhibitors (ICIs) do not ensure complete satisfactory outcome in patients[18, 19, 20]; therefore, the discovery of novel inhibitory receptors would have significant scientific and clinical implications, since they can be ideal targets for cancer immunotherapy.

The term IS originated from synapse of the nervous system that shares similar properties of cell-to-cell contact and signal transmission[21]. Guidance cues, including attractive and repulsive cues, are the key molecules regulating axonal outgrowth and synapse formation in the central nerve system (CNS)[22, 23]. Among the many repulsive cues that function as inhibitors for axon growth and synaptic function, the role of Nogo receptor 1 (NgR1) in neurophysiopathology has been well established[24, 25, 26]. NgR1 recognizes its ligand, NogoA, and induces neuronal degeneration by RhoA signal that regulates actin cytoskeletal dynamics in damaged neurons[27, 28]. NgR1 is also expressed in various immune cells and regulates their adhesion to myelin expressing NogoA, suggesting an immunomodulatory role of it in neuroinflammation[29, 30]. However, the studies are limited to the nervous system, providing insufficient molecular mechanisms, and do not address the role of NgR1 in tumor control, which is a crucial function of immune cells. Therefore, defining the role of NgR1 in the IS formation and subsequent

killing effects of NK cells is necessary to improve the understanding of the antitumor mechanism of NK cells.

In this study, we reported the modulatory role of NgR1, interfering with contact stability and complete IS formation, in the killing effects of NK cells on NogoA-expressing target cells. Moreover, the relationship between NogoA expression in tumors and NK cell infiltration indicated unfavorable clinical outcomes in patients. Taken together, the findings revealed the underlying mechanism of regulation of IS formation by NgR1, suggesting its potential in improving cancer immunotherapy.

## Results

### NgR1 interferes with the antitumor effects of NK cells

To assess the role of NgR1 in NK cells, we first investigated the cell surface expression of NgR1. We found NgR1 to be expressed in mouse primary NK cells, CD8 T cells, and EL4 cell line (Fig. 1a and Extended Data Fig. 1a). Since NK cells recognize the ligand and lyse cancer cells[3, 7], we confirmed the expression of NogoA, a ligand of NgR1, in various cancer cell lines (Extended Data Fig. 1b). Next, we measured the cell-mediated cytotoxicity of mouse splenocytes to investigate the involvement of NgR1 in the cytolytic function of immune cells. With NEP1-40 treatment, which is an antagonistic peptide of NgR1[31], splenocytes of wild type (WT) mice showed higher cytotoxicity than those in control group (Fig. 1b and Extended Data Fig. 1c). Moreover, we found splenocytes from NgR1 knocked out (KO) mice to exhibit higher cytolytic effects than those from WT mice (Fig. 1c). To verify the specificity of NEP1-40 and whether the function of NgR1 is restricted to NK cells, we investigated the cytotoxicity of NK cells isolated from the spleens of WT and KO mice with or without NEP1-40 treatment. NK cells from KO mice showed higher cytotoxicity than those from WT mice, and only NK cells from WT mice showed increased cytotoxicity with NEP1-40 treatment (Fig. 1d). Since NK cytotoxicity improved upon NgR1 deficiency, we hypothesized that WT and KO mice would exhibit different resistance to tumors. To verify the same, a syngeneic mouse model of lung metastasis was established for WT and KO mice (Fig. 1e). After intravenous (i.v.) administration of B16F10 cells, fewer metastatic nodules remained in the lungs of KO mice than in WT, but no difference was seen in the NK cell-depleted group, suggesting that the animal model was NK cell-dependent (Fig. 1f and g). Since NK cell infiltration in tumors is an

indicator of tumor resistance[32, 33], we investigated the population of intrapulmonary NK cells. The NK cell population ($CD3^-NK1.1^+$) that infiltrated into the lungs bearing tumor nodules was higher in KO mice than in WT (Fig. 1h). The data suggested that NgR1 in NK cells contributes negatively to tumor control.

To investigate whether the improved antitumor effect caused by NgR1 deficiency is due to intrinsic alterations in immune composition, we analyzed the population of immune cells from both WT and KO mice. Total NK cells ($CD3^-NK1.1^+$) were classified into 4 maturation stages, according to the expression of CD11b and CD27, namely immature NK cells ($CD27^-CD11b^-$), early mature NK cells ($CD27^+CD11b^-$), mature NK cells ($CD27^+CD11b^+$), and late mature NK cells ($CD27^-CD11b^+$)[34]. We found no difference between WT and KO mice in resting and IL-2-stimulated total or classified NK cell populations, as well as in IFNγ expression (Extended Data Fig. 2a-c). Populations of CD8 T cells ($CD3^+CD8^+$), CD4 T cells ($CD3^+CD4^+$), B cells ($B220^+$), myeloid cells ($CD11b^+Gr1^+$), neutrophils ($CD11b^+Gr1^{high}$), monocytes ($CD11b^+Gr1^{low}$), and macrophages ($CD11b^+F4/80^{high}$) were also not different in WT and KO mice (Extended Data Fig. 2d-f). The data collectively indicated that NgR1 deficiency does not affect the composition of immune cells, implying that NgR1 is mainly involved in the effector function of NK cells.

## NgR1 regulates the actin cytoskeleton dynamics of NK cells

Since NgR1 is involved in the tumor control of mouse NK cells, it might play a prominent role in human NK cells as well. To verify this, we investigated the expression of NgR1 and its signals in human NK cells. NgR1 was found to be expressed in human NK cells, including umbilical cord blood (UCB)-derived NK cells (UCB-NK), cytokine-induced matured NK cells (mNK), NK92 cell line, UCB-CD8 T cells, and Jurkat cell line (Fig. 2a and Extended Data Fig. 3a). Since the GPI-anchored receptor, NgR1, lacks an endo-domain for intracellular signaling, it requires the participation of a complex of co-receptors, including immunoglobulin-like domain-containing protein 1 (LINGO1), tumor necrosis factor receptor superfamily member 19 (TROY), and neutrophin receptor (p75NTR)[35, 36]. We found the co-receptors of NgR1 to be expressed in NK92, Jurkat, and EL4 cell lines (Extended Data Fig. 3b). NgR1 is well known to recognize NogoA, and activates cytoskeleton-regulatory signals[27, 37]. With RhoA activation by NgR1 stimulation, Rho-associated coiled-coil-containing protein kinase (ROCK) phosphorylates LIM domain kinase 1 (LIMK) to phosphorylate and inactivate cofilin, which

severs filamentous (F)-actin into globular (G)-actin[25, 26, 27]. To investigate the signaling of NgR1, we stimulated NgR1 in NK cells. By treatment with Nogo-P4, an agonistic peptide of NgR1[38], both RhoA and LIMK were activated, and cofilin was inactivated in NK92 cells and UCB-NK cells (Fig. 2b and Extended Data Fig. 3c). RhoA activation promotes stress fiber formation through actomyosin-based contraction and cofilin inactivation, leading to actin cytoskeleton reorganization[39, 40]. Accumulation of F-actin causes the formation of cell membrane protrusion, which affects cell migration and adhesion[41, 42]. Since NgR1 stimulation activates RhoA and inactivates cofilin, we hypothesized that NgR1 would affect the actin regulation of NK cells. To verify this, F-actin was directly visualized in NK92 cells expressing Lifeact-GFP, and the effects of Nogo-P4 treatment on F-actin dynamics were assessed by video microscopy. Nogo-P4-treated NK92 cells exhibited significantly increased F-actin intensity (Fig. 2c, d, and Supplementary Video 1) and membrane protrusion frequency (Fig. 2c, e, and Supplementary Video 1) compared to untreated (Ctrl) or scrambled peptide (Scram)-treated NK cells. The data suggested that NgR1 in NK cells regulates actin cytoskeleton dynamics through the RhoA signal.

## NgR1 regulates NK cell-mediated killing specifically for NogoA

To assess the NogoA-specificity of NgR1 in NK cell killing, we investigated NK cell-mediated cytotoxicity by regulating the function and expression of NgR1 in NK cells or NogoA in target cells. First, we confirmed the expression of NogoA in cancer cell lines. NogoA was expressed at different levels on the surface of the target cells (Extended Data Fig. 4a). Killing of NK92 cells relative to K562, which hardly expressed NogoA, showed no difference with or without blocking NgR1 with NEP1-40 (Fig. 3a). However, NK-mediated killing was significantly reduced for NogoA-overexpressing K562 cells and was rescued by NEP1-40 treatment, similar to that in HEK293T cells (Fig. 3b, c, and Extended Data Fig. 4b and c). By treating NEP1-40, NK cytotoxicity increased against U87MG cells, a glioma cell line from brain tumors known to express high levels of NogoA[43] (Fig. 3d). We further found that NK cytotoxicity increased upon inhibiting NogoA expression in U87MG cells or NgR1 expression in NK92 cells (Fig. 3e, f, and Extended Data Fig. 3d and e). Since NK cell activity depends on the balance between activating and inhibitory signals to kill the target[3, 6, 17], we questioned whether NgR1 could be involved in killing NK cell-resistant targets. To verify this, we investigated the expression of activating and inhibitory ligands in several cell lines. Among them, AU565 cells expressed NogoA while expressing little or no activating ligand, such as

ULBP1, ULBP2, ULBP3, and MIC-A/B (Extended Data Fig. 4a and f). The cytotoxicity of NK cells against AU565 cells significantly increased due to the blocking of NgR1 by NEP1-40 treatment (Fig. 3g). Like NK92 cells, human mNK cells also showed increased killing upon blocking NgR1 (Extended Data Fig. 4g). Therefore, the data collectively suggested that NgR1 acts as an inhibitor for the cytolytic function of NK cells, specifically in presence of NogoA.

## NK-to-target cell contact is destabilized by NgR1

To further gain insight into how NgR1 signaling inhibits NK cell cytotoxicity, we directly observed interactions between NK and target cells by live-cell imaging. Most of the control NK92 cells transiently interacted with U87MG cells (top panel of Fig. 4a and Supplementary Video 2), whereas a large fraction of NEPI-40-treated NK92 cells made stable contact with U87MG cells and some NK92 cells eventually killed U87MG cells (bottom panel of Fig. 4a and Supplementary Video 2). Typically, NK cells transiently interact with target cells to scan their surfaces (step I in Fig. 4b) and then form stable synapses (step II in Fig. 4b) that direct the polarized secretion of lytic granules to perform target cell lysis (step III in Fig. 4b). We analyzed the percentage of NK92 cells transiently interacting with target cells with a contact duration < 10 min (Fig. 4c), and measured the contact duration between NK92 cells and target cells forming stable synapses (Fig. 4d). NEP1-40-treatment was found to significantly reduce transient interactions and increase contact duration, resulting in enhanced cytotoxicity (Fig. 4e). Similar results were obtained with mouse NK cells when NgR1 was either blocked by NEP1-40 (Extend Data Fig. 5a-d and Supplemetary Video 3) or genetically knocked out (Extend Data Fig. 5e-h and Supplemetary Video 4). Together, the results indicated that NgR1 signaling reduces NK cell cytotoxicity by interfering with stable synapse formation.

## F-actin dynamics in NK cells is regulated during IS formation by NgR1

NgR1 signaling is responsible for altering the actin cytoskeletal balance[25, 27, 37]. To investigate the NK-to-target contact by the molecular mechanism of NgR1 downstream signals, we regulated cofilin expression or LIMK activity (Fig. 5a). Since cofilin directly regulates F-actin dynamics[27, 39, 40], we hypothesized that inhibition of cofilin expression would affect F-actin turnover, resulting in impairment of NK cell contact and subsequent killing. To verify this, we suppressed the expression of cofilin in NK92 cells with siRNA (Extended Data Fig. 6a), and found that NK92-U87MG conjugation was reduced and NK killing was impaired (Fig.

5b and c). Next, we investigated NK-to-target contact and NK killing by treating NK cells with LIMKi3 (LIMK inhibitor). Nogo-P4-treated NK92 cells increased phosphorylation of LIMK and cofilin, whereas LIMKi3 treatment inhibited both LIMK phosphorylation and subsequent cofilin phosphorylation (Extended Data Fig. 6b). Moreover, we found inhibition of LIMK and cofilin phosphorylation to occur through LIMK inhibition under NogoA-expressing U87MG cell-mediated NgR1 stimulation of NK92 cells (Fig. 5d). The contact between NK92 and U87MG cells following inhibition of LIMK was directly observed via live-cell imaging. Similar to NgR1 blockade or KO, LIMKi3 treatment significantly stabilized NK-target contacts, leading to enhanced cytotoxicity of NK cells (Fig. 5e-h and Supplementary Video 5).

Next, we visualized F-actin dynamics in the context of IS using NK92 cells expressing Lifeact-GFP. F-actin polymerization at the IS is one of the early events critical for stable IS formation[8, 9, 10, 11, 13, 14]. In the control group, NK92 cells contacting U87MG cells mainly polarized F-actin outward from NK-to-target contacts and frequently detached from the target cells (top panel of Fig. 6a and Supplementary Video 6). In contrast, NEP1-40-treated NK92 cells polarized F-actin toward the NK-to-target contacts and maintained stable IS formation (bottom panel of Fig. 6a and Supplementary Video 6). F-actin distributions with respect to NK-to-target contacts were classified into 4 cases and were plotted for NK92-U87MG conjugates after the initiation of co-culture (Fig. 6b). In the control group, majority of NK92 cells polarized F-actin outward from the NK-to-target contacts, whereas in the NEP1-40-treated group, most NK92 cells polarized F-actin toward the NK-target contacts (Fig. 6b). NgR1 signaling also influenced lytic granule convergence and polarization toward the NK-target contacts, both of which are critical events for cytotoxicity (Fig. 6c-d and Supplementary Video 7); majority of NK92 cells in the control group exhibited diffuse patterns of granules, indicating their failure to converge the granules. In contrast, most NK92 cells treated with NEP1-40 converged the lytic granules to the distal pole (approximately 50% in 30 min), and then polarized them toward the IS (approximately 80% in 120 min). The results together indicated that suppressed F-actin dynamics, mediated by NgR1 signaling at the NK-to-target contacts, promote F-actin polymerization outward from the cell-to-cell contacts, resulting in the detachment of NK92 cells prior to lytic granule polarization towards IS.

## NgR1 functions as an immune checkpoint in NK cells

Considering that NK cells perform immune surveillance and NgR1 inhibits the cytolytic function of NK cells, the therapeutic effect of NgR1 blockade was investigated using a xenograft mouse model. Following subcutaneous injection of U87MG cells, NSIG mice were intravenously injected with NK92 cells on days 10 and days 14, and scrambled peptide or NEP1-40 was injected intratumorally on days 11 and days 15 (Fig. 7a). Tumor size was decreased in the group administered NK92 cells + NEP1-40 compared to that in the group injected with PBS (control) and NK92 cells + scrambled peptide (Fig. 7b and c). Survival rate of tumor-bearing mice was improved in the group administered NK92 cells + NEP1-40 (Fig. 7d). We next assessed whether NgR1 could be linked to clinical outcomes alongwith a relationship with *RTN4*, Nogo gene, in patients with cancer. First, rich- or poor-NK-infiltrated groups were divided using CIBERSORT, and then clinical prognosis was deduced by grouping of patients with high or low *RTN4* expression in TCGA pan-cancer data (Fig. 7e). In all cancer patients, regardless of the quantity of infiltrated NK cells, we confirmed that *RTN4* is a risk factor for survival and that high *RTN4* leads to poor clinical outcomes. (Fig. 7f and g, Extended Data Fig. 7a and Supplementary Table 1). In particular, the *RTN4* expression level of NK-rich patients showed a higher risk for overall survival than NK-poor patients. Like NK cells, CD8 T cells also showed similar results in clinical outcomes and risk analysis for survival (Extended Data Fig. 7b-d and Supplementary Table 2). Collectively, the data suggested that NgR1 of cytolytic immune cells serves as an immune checkpoint to inhibit IS formation, and is a novel therapeutic target for controlling tumors (Fig. 7h).

## Discussion

In this study, we identified NgR1 as a novel NK cell inhibitory receptor prohibiting stable IS formation by LIMK-cofilin-mediated alteration of actin dynamics. NgR1 deficiency or blockade promoted the stable formation of IS, thereby increasing NK cell killing and tumor control. Even when NK cells were infiltrated, patients with cancer expressing abundant Nogo still had poor prognosis. This revealed the underlying mechanism of improvement of NK cell function by NgR1 and highlighted the clinical finding that NgR1 acts as an immune checkpoint.

In the CNS, axonal growth and synapse formation are critical for signal transmission of neurons. In contrast to attractive cues promoting axon outgrowth and synapse formation by Rac1, and CDC42 signals promoting cytoskeleton dynamics, inhibitory cues interfere with axonal growth and synaptic function by RhoA signals suppressing cytoskeleton remodeling[22,

[23]. Neuronal growth inhibitors interfere with synapse formation by inducing axon growth cone collapse and retraction[22, 23, 26]. Among the inhibitors, NogoA-NgR1 interaction, which belongs to myelin-associated inhibitor, inhibits axonal growth and synaptic function through RhoA-mediated cyosketon regulation and is required to prevent abnormal neuronal sprouting in healthy brain and for neuronal degeneration upon CNS damage[25, 26, 28, 37]. NgR1 acts as an inhibitory receptor that directly regulates neurons rather than blocking signals of attractive cues[44, 45]. Recently, NgR1 has been reported to inhibit the adhesion of immune cells[46]; however, this is restricted to the nervous system and detailed mechanisms are missing. Elucidating the role of NgR1, which is otherwise well-defined in the nervous system, for tumor control by immune cells would be necessary for understanding the mechanism of action of immune cells better, thereby contributing to the satisfactory performance of cancer immunotherapy.

NK cells form IS with target cells in order to identify infected/transformed cells and exert cytotoxicity. Synapse-mediated cytotoxicity is accomplished via stepwise processes, including tethering, F-actin accumulation, firm adhesion, granule convergence to MTOC, MTOC polarization to IS, and granule exocytosis[10, 11]. Signaling mediated by inhibitory receptors, such as NKG2A and KIR, acts primarily in the early stages of IS to prevent activating signals from occuring[11, 17]. Functionally, inhibitory receptor signals destabilize the IS, and promote NK cell detachment and migration[47, 48]. The characteristics of NgR1-mediated NK cell inhibition, observed in this study, were similar to those of inhibitory receptors; in presence of NgR1-NogoA interactions, NK cells exhibited transient interactions with target cells and failed to polarize F-actin and lytic granules toward the IS, resulting in impaired cytotoxicity. However, NgR1 is distinct from other inhibitory receptors due to the downstream signals that it triggers. Typically, inhibitory receptors recognize either major histocompatibility complex class I (MHC I) or non-MHC I ligands and signal through immunoreceptor tyrosin-based inhibitory motifs (ITIMs) located at their cytoplasmic tails, thereby blocking the activating signals[17, 20]. NgR1, on the other hand, interacts with NogoA and signals RhoA through co-receptors, since it is a GPI-anchored receptor with no cytoplasmic domain[25, 37]. Recently, ICIs have been developed to improve the tumor-killing ability of immune cells; however, issues such as application to specific cancer types, recurrence, or resistance still exist[18, 19, 20]. It is not yet clear whether blocking the activating signals through ITIMs is the only mechanism that regulates actin dynamics and prevents IS formation in the NK cells[15]. Therefore, the discovery of NgR1 as an inhibitory receptor broadens the range of NK inhibitory receptors.

Although the role of actin cytoskeleton remodeling mediated by the RhoA-ROCK-LIMK-cofilin axis, downstream of NgR1 signaling, has been well established in neural synapse[25, 26, 28, 37], it has not been investigated in IS. While RhoA-mediated inhibition of T cell and NK cell cytotoxicity[49, 50] and cofilin-mediated T cell synapse formation for T cell activation[50, 51] had previously been reported, upstream signals activating RhoA and deactivating cofilin have not been identified yet. For ITIM-mediated actin remodeling in NK cells that leads to synaptic destabilization, dephosphorylation of Vav1[52], a guanine nucleotide exchange factor important for immune cell activation, and phosphorylation of the adaptor protein Crk[53] have primarily been considered[15]. It would be interesting to see whether the pathway identified in this study is also triggered in ITIM-mediated NK cell suppression. Overall, our preliminary results revealed that CD8+ T cells express NgR1, and NgR1-mediated signaling inhibited T cell-mediated cytotoxicity, implying that NgR1 could be a crucial inhibitory checkpoint for our immune system.

## Methods

### Ethics

This study complies with all applicable codes of ethics. Human studies were approved by the KIRBB Institutional Review Board (P01-201610-31-002). For the use of human umbilical cord blood (UCB), informed consent was obtained from the donor through the Cord Blood Bank of Korea. Animal studies were approved by the Animal Experimental Ethics Committee (AEC-21016, -21017) and conformed to the Regulations on the management and use of laboratory animals of KRIBB.

### Mice

All mice were bred and/or maintained in the specific-pathogen-free (SPF) animal facility with 22–26 ℃ and 40–60% humidity on a 12-h dark–light cycle in the Laboratory Animal Resource Center at KRIBB. C57BL/6N mice (wild type, WT) purchased from DooYeol Biotech, NgR1 KO (KO) mice (C57BL/6-Rtn4r$^{tm1cyagen}$) purchased from Cyagen Biosciences Inc., NSIG mice purchased from GHBIO were used for expreiments at 6–8 weeks of age. Male mice were used for in vitro studies and experiments on antitumor effects in vivo. All animal experiments were performed in agreement with the Animal Experimental Ethics Committee of KRIBB.

## Primary NK cell preparation

WT and KO mice were used in vitro experiments for splenocytes harvesting and NK cell isolation. Splenocytes were recovered by grinding the spleen of mice with 70-μm Cell Strainer (SPL Life Sciences). NK cell were isolated from splenocytes using an NK Cell Isolation Kit, mouse (Miltenyi Biotec). Isolated NK cells were cultured in RPMI 1640 (Gibco) containing 10% FBS, 1% penicillin/streptomycin and 10 ng/ml recombinant human IL-2 (hIL-2) (PeproTech). Human umbilical cord blood (UCB) were used for NK cell isolation. UCB-derived NK cells (UCB-NK) were isolated using $CD3^+$ cell depletion with Rosette Sep (StemCell Technologies), density separation with Lymphoprep (StemCell Technologies) and enrichment with NK Cell Isolation Kit, human (Miltenyi Biotec). Cytokine-induced matured NK cells (mNK) were differentiated from CD34+ hematopoietic stem cells (HSCs). Human $CD34^+$ HSCs were isolated from UCB using Rosette Sep, Lymphoprep and CD34 MicroBead Kit, human (Miltenyi Biotec). NK cell precursors (pNK) were differentiated from CD34+ HSC in Myelocult H5100 (StemCell Technologies) supplemented with Hydrocortisol ($10^{-6}$M), SCF (30 ng/ml), Flt3 (50 ng/ml) ligand and IL-7 (5 ng/ml) for 14 days. Mature NK cells were differentiated from pNK cells by stimulation with Hydrocortisol ($10^{-6}$M), IL-21 (30 ng/ml) and IL-15 (30 ng/ml) for 14 days. Primary NK cell of mouse and human were maintained under 37 ℃ and humidified 5% $CO_2$ conditions.

## Cell lines

YAC-1, CT26, 4T1, B16F10, Jurkat, EL4, AU565 and K562 cells were cultured in RPMI 1640 (WelGENE) supplemented with 10% fetal bovine serum (FBS) and 1% penicillin/streptomycin (Gibco). NK92 cells were cultured in alpha-MEM (WelGENE) supplemented with 10% FBS, 1% penicillin/streptomycin and hIL-2 (10 ng/ml). HEK293T cells were cultured in DMEM (WelGENE) supplemented with 10% FBS and 1% penicillin/streptomycin. U87MG cells were cultured in MEM (WelGENE) supplemented with 10% FBS and 1% penicillin/streptomycin. Cells were incubated at 37 ℃ and humidified 5% $CO_2$ conditions.

## Flow cytometry analysis

Cells were washed and stained with antibodies in PBS containing 1% FBS and 2 mM EDTA for 20-30 min in the dark at 4 ℃. The following antibodies and dilutions were used for

detection of cell surface expression: anti-NgR1-Alexa 647, anti-NK1.1-APC, anti-CD3-Amcyan, anti-CD27-PE, anti-CD11b-PE-Cy7, anti-CD8-PE-Cy7, anti-B220-Pacific Blue, anti-Gr1-Pacific Blue, anti-F4/80-APC, anti-ULBP1-FITC, anti-ULBP2-APC, anti-ULBP3-PE, anti-MIC-A/B-PE, anti-HLA-A/B/C-FITC, anti-p75NTR-FITC. For intracellular IFN-γ staining, cells were fixed and permeabilized using a Fixation/Permeabilization kit (BD Biosciences) after surface staining, and labeled with anti-IFN-γ-PE-Cy7 for 20-40 min in the dark at 4 ℃. The fluorescent dyes were conjugated to anti-NgR1, anti-LIGO1, and anti-TROY using Alexa Fluor™ 647 Antibody Labeling Kit (Invitrogen) for flow cytometry analysis of dye-uncojugated antibodies. Isotype controls containing anti-IgG-APC and anti-IgG-FITC were used as negative controls. Antibody-labeled cells were analyzed by a fluorescence-activated cell sorter (FACS) Canto II (BD Biosciences) and data were collected using FlowJo software (Tree Star).

### Cytotoxicity assay

NK cell-mediated cytotoxicity was measured using a calcein-AM relase assay. Target cells were incubated with calcein-AM (Invitrogen) for 1-h at 37℃ and humidified 5% $CO_2$ conditions. Calcein-labled taret cells were plated into a 96-well round-bottom plates and then co-cultured with serially diluted effector cells at the designed Effector (E):Target (T) ratio for the desiered incubation time. The calcein-relase from lysed trarget cells into supernatants by the effector cells was measured using a multimode microplate reader (Molecular Devices). Maximal and spontaneous release of calcein was simulated by adding 2% Triton X-100 and complete medium to calcein-labeled target cells, respectively. The percentage of specific lysis was calculated using the formula: (experimental release – spontaneous release)/(maximum release – spontaneous release) × 100%. NEP1-40 or anti-NgR1 was treated during co-culture of effector and target cells to block NgR1.

### Lung metastatic syngeneic mouse model

A lung metastasis model using the B16F10 melanoma cell line was constructed in WT and KO mice. For depletion of NK cells in mice, 100 ug of anti-NK1.1 or isotype control in 200 ul DPBS were injected intravenously through tail of mice 4 days and 1 day before, and 2 days after intravenouse (i.v.) injection of B16F10. The $CD3^-NK1.1^+$ populations were measured by flow cytometry analysis 5 days before, 4 days and 13 days after B16F10 injection. Each mouse

was injected intravenously with $2 \times 10^5$ B16F10 cells on day 0. The body weight of the mice was measured on days 0, 9 and 14 after injection of B16F10 injection. Mice were sacrificed 14 days after injection of cancer cells, and lungs were removed from mice to analyze the metastatic melanoma nodules. The removed lungs were ground with a 70-μm Cell Strainer to analyze the intrapulmonary $CD3^-NK1.1^+$ population by flow cytometry.

## Cell line derived tumor xenograft mouse model

A Xenograft model using human U87MG glioblastoma cell line was establihed in NSIG mice lacking T cells, B cells and NK cells. For the development of solid tumors, $4 \times 10^6$ U87MG cells were implanted subcutaneously into mice on day 0. NK92 cells ($2.5 \times 10^5$) were injected intravenously through the tail of mice 10 and 14 days after U87MG injection, and 300 ug of scrambled peptide (Scram) or NEP1-40 in 100 ul DPBS were injected intratumorally on days 11 and 15. In the control group (Ctrl) inoculated with only U87MG cells, without NK92 cells, intratumoral (i.t.) injection of 100 ul DPBS were applied. From 10 days after plantation of the tumor cells, the width and length of the developed tumor were measured every 4 days with a caliper to calculate the tumor size ($mm^3$): $(\text{width} + \text{length})^2/2$, and the body wieght was also measured at the same time. After tumor development, survivals of mice were monitors every days during the entire experimental period.

## Immunoblotting

Cells were washed with ice-cold PBS and lysed using cOmplete™ Lysis-M (Rhoche) and protein concentrations were measured with a Pierce™ BCA Protein Assay Kit (Thermo Scientific). The cell lysates containing 10-20 ug of proteins were reduced by boiling for 10-15 min using SDS sample buffer. Samples were separated by 8-12% sodium dodecyl sulfate (SDS)-polyacrylamide gel electrophoresis (PAGE) gels and transferred to a polyvinylidene fluoride membrane (Millipore). Membranes were blocked with 1-5% nonfat milk or BSA in PBS containing 0.05 % Tween 20 (Duchefa Biochemie) for 40-60 min at room temperature and then incubated with primary antibodies overnight at at 4 °C. Membranes were then washed and icubaed with horseradish peroxidase (HRP)-conjugated anti-rabbit or anti-mouse IgG secondary antibody for 40-60 min at room temperature. After washing, the membranes were developed using SuperSignal™ West Pico PLUS Chemiluminescent Substrate (Thermo Scientific) and immunoblotting images were obtained using WSE-6100 LuminoGraph (ATTO).

Data were collected using CASanalyzer (ATTO) software. For endegenous RhoA-GTP detection, cells were lysed using cOmplete™ Lysis-M, and cell lysates were pulled down using Rho Activation Assay Biochem Kit™ (Cytoskeleton) according to the manufacturer`s protocol. Cell lysates were incubated with Rhotekin, a Rho effector protein that has a Rho binding domain (RBD) and is tagged with GST, in a rocker at 4 ℃ for 1 h. Centrifuged and washed samples were reduced by boiling for 10-15 min using SDS sample buffer, and followed by separation and transfer. The following antibodies and dilutions were used: anti-pLIMK2, anti-LIMK2, anti-pCRMP2, anti-CRMP2, anti-pCofilin, anti-Cofilin, anti-GAPDH, anti-NogoA, anti-NgR1, anti-rabbit IgG-HRP and anti-mouse IgG-HRP.

## Establishment of stable cell lines

Lifeact-EGFP was transduced into NK92 cells using a lentiviral system for microscopic visual measurement of F-actin in NK cells. For lentivirus generation, HEK293T cells were plated the day before lipoplex-mediated transfection. A mixture of pLenti Lifeact-EGFP (Addgene), VSV-G, pMDLg/pRRE, pRSV-Rev (3:1:1:1 ratio) and TransIT®-2020 Transfection Reagent (Mirus) in Opti-MEM™ I (Gibco) containing 1% penicillin/streptomycin was treated to HEK293T cells in a droplet manner, and cultured for 3 days in RPMI 1640 supplemented with 10% (FBS) and 1% penicillin/streptomycin. The collected supernatants were centrifuged, filtered through a 0.45 um filter, and resuspended in medium after ultracentrifugation. NK92 cells were infected with titrated virus and protamin sulfate in alpha-MEM supplemented with 10% FBS, 1% penicillin/streptomycin and hIL-2 (10 ng/ml), and incubated for 3 days at 37 ℃ and humidified 5% $CO_2$ conditions. Lentivirus-infected and uninfected NK92 cells were selected by blasticidin.

## Transient transfection

K562 cells overexpressed NogoA using electroporation. K562 cells ($10^6$) and 2.5 ug of pCMV Nogo-A (OriGene) in 100 ul of Opti-MEM™ I containing 1% penicillin/streptomycin were loaded into NEPA Electroporation Cuvettes (Nepa Gene). After electroporation using NEPA21 Type II (Nepa Gene), according to the manufacturer`s protocol, K562 cells were cultured in RPMI 1640 supplemented with 10% FBS and 1% penicillin/streptomycin at 37 ℃ and humidified 5% $CO_2$ conditions for 2-3 days. NogoA overexpressed K562 cells were analyzed for NogoA expression using immunoblotting and flow cytometry assay and applied

to cytotoxicity assay. HEK293T cells overexpressed NogoA using lipoplex-mediated transfetion. HEK293T cells were plated one day before transfection and prepared at a density of about 70% on the day of transfection. A mixture of pCMV NogoA and TransIT®-2020 Transfection Reagent in Opti-MEM™ I containing 1% penicillin/streptomycin was treated to HEK293T cells by droplet manner. After 2-3 days, the expresion level of NogoA overexpressed in HEK293T cells was analyzed by immunoblotting and flow cytometry, and these cells were used for cytotoxicity assay. In U87MG cells, NogoA was knocked down using small interfering RNA (siRNA) through lipoplex-mediated transfetion. U87MG cells plated one day before transfection were treated with a mixture of siRNA for NogoA (siNogoA) and TransIT-X2® Dynamic Delivery System (Mirus) in Opti-MEM™ I. Transfected U87MG cells were cultured in DMEM supplemented with 10% FBS and 1% penicillin/streptomycin at 37 ℃ and humidified 5% $CO_2$ conditions for 2-3 days. NogoA expression in U87MG cells was analyzed using immunoblotting and U87MG cells in which NogoA was knocked down were used for cytotoxicity assay. In NK92 cells, NgR1 or Cofilin was knocked down by electroporation. NK92 cells ($10^6$) and 10 uM of siNgR1 or siCofilin in 100 ul of Opti-MEM™ I containing 1% penicillin/streptomycin were loaded into NEPA Electroporation Cuvettes. NK92 cells electroporated with NEPA21 Type II were cultured in alpha-MEM supplemented with 10% FBS, 1% penicillin/streptomycin and hIL-2 (10 ng/ml) at 37 ℃ and humidified 5% $CO_2$ conditions. After 2-3 days, the expression level of NgR1 or Cofilin knocked down in NK92 cells was analyzed using immunoblotting or flow cytometry, and these cells were used for cytotoxicity assay. The siRNA sequences are as follows: siNogoA, 5'-GAUUGAAGCGCAAAGCUGA-3'; siNgR1 #1, 5'-CGTGACCTCAAACGCCTAGCTGCCAATGA-3'; siNgR1 #3, 5'-AGCCTCGACCGTCTCCTACTGCACCAGAA-3'; siCofilin, 5'-GUGUAUAAAUGGAAUGUUG -3' (Bioneer).

## Enzyme-linked immunosorbent assay (ELISA)

The supernatants of the cytotoxicity assay were used in the cytokine ELISA. Human IFN-γ and TNF-α ELISA kits were purchased from eBioscience and performed according to the manufacturer's protocol.

## Live cell imaging

A modified Olympus IX 83 epi-fluorescence microscope with a 40X (UPlanFLN, NA=1.30) objective lens and an ANDOR Zyla 4.2 sCOMS camera was used for imaging experiments. The microscope was automatically controlled by Micro-manager. For live cell imaging, the microscope stage was equipped with a Chamlide TC incubator system (Live Cell Instrument, Korea) maintaining a cell culture condition (37 ℃, $CO_2$ 5 %). Acquired images were processed using ImageJ. To observe F-actin dynamics in NK92 cells, NK92 cells expressing Lifeact-GFP were seeded, and time-lapse imaging acquiring differential interference contrast (DIC) and GFP fluorescecne was initiated about 15 min after cell seeding. To observe NK cell-cancer cell interactions, cancer cells were first plated on gelatin-coated coverslips and incubated for 12 h in a tissue culture incubator (37℃ with 5% CO2) so that cancer cells adhere and spread on the substrates. Then, the coverslip containg cancer cells was mounted in a magnetic chamber (Chamlide CF, Live cell Instrument, Korea), and the chamber was loaded on the microscope stage equipped with the incubator system. NK cells were added in the chamber, and time-lapse imaging was initiated 15 min after NK cell addition to allow NK cells to sediment and initiate interactions with the cancer cells. To visualize F-actin and lytic granules, NK cells transfected with Lifeact-GFP and labeled with lysosensor (Thermo Fisher) were used, respectively. Killing probability were measured by time-lapse image. Total interaction events and killed target cells were directly counted at each Field of View (FOV). Killing probability = $\frac{\#\ of\ killing}{total\ \#\ of\ interactions}$

## Patient samples

Gene expression and clinical information were downloaded from the GDC data portal (https://portal.gdc.cancer.gov). The 9,473 primary tumors of The Cancer Genome Atlas (TCGA) with 33 cancer types included ACC, BLCA, BRCA, CESC, CHOL, COAD, DLBC, ESCA, GBM, HNSC, KICH, KIRC, KIRP, LAML, LGG, LIHC, LUAD, LUSC, MESO, OV, PAAD, PCPG, PRAD, READ, SARC, SKCM, STAD, TGCT, THCA, THYM, UCEC, UCS, and UVM, were used for survival analysis. The log2 scaled FPKM values were used for analyzing gene expression.

## CIBERSORT

CIBERSORT was used for the mathematical analysis of the pan-cancer of gene expression (https://cibersort.stanford.edu)[54]. We used log2 scaled FPKM values for deconvolution analysis of available gene expression levels[55]. The created gene expression file with the 9,574

cases was uploaded to CIBERSORT as a mixture file, and CIBERSORT was run with options for LM22 reference file, 500 permutations, and quantile normalization disabled. The quantity of NK cell was produced by the sum of the quantity of activated NK cells and resting NK cells in the LM22 reference file. The samples, which were the quantity of NK cells or CD8 T cells in the top 10% to 50% with statistical significance ($P < 0.05$), were included in NK or CD8 T rich group, and the others were included in poor group.

## Statistical and survival analysis

The one-way or two-way ANOVA with Tukey`s or Sidak`s multiple-comparisons test or unpaired two-tailed Student`s *t*-test was used to analyze the significance of data using GraphPad Prism. The log-rank test and Cox hazard models with 95% CIs were performed to estimate the significance of the overall survival. The Kaplan-Meier plot and forest plot were performed to visualize. All survival analyses of clinical information were used by R software package (ver. 3.6.3). Statistical values are NS, not significant ($P > 0.05$); *$P < 0.05$; **$P < 0.01$; ***$P < 0.001$; ****$P < 0.0001$. Data are represented as mean ± s.d. or s.e.m.

## References


1. Smyth, M.J., Godfrey, D.I. & Trapani, J.A. A fresh look at tumor immunosurveillance and immunotherapy. *Nat Immunol* **2**, 293-299 (2001).

2. Hiam-Galvez, K.J., Allen, B.M. & Spitzer, M.H. Systemic immunity in cancer. *Nat Rev Cancer* **21**, 345-359 (2021).

3. Guillerey, C., Huntington, N.D. & Smyth, M.J. Targeting natural killer cells in cancer immunotherapy. *Nat Immunol* **17**, 1025-1036 (2016).

4. Liu, S.*, et al.* NK cell-based cancer immunotherapy: from basic biology to clinical development. *J Hematol Oncol* **14**, 7 (2021).

5. Trinchieri, G. Biology of natural killer cells. *Adv Immunol* **47**, 187-376 (1989).

6. Cerwenka, A. & Lanier, L.L. Natural killer cells, viruses and cancer. *Nat Rev Immunol* **1**, 41-49 (2001).

7. Vivier, E., Tomasello, E., Baratin, M., Walzer, T. & Ugolini, S. Functions of natural killer cells. *Nat Immunol* **9**, 503-510 (2008).

8. Davis, D.M.*, et al.* The human natural killer cell immune synapse. *Proc Natl Acad Sci U S A* **96**, 15062-15067 (1999).

9. Davis, D.M. Assembly of the immunological synapse for T cells and NK cells. *Trends Immunol* **23**, 356-363 (2002).

10. Orange, J.S. Formation and function of the lytic NK-cell immunological synapse. *Nat Rev Immunol* **8**, 713-725 (2008).

11. Mace, E.M.*, et al.* Cell biological steps and checkpoints in accessing NK cell cytotoxicity. *Immunol Cell Biol* **92**, 245-255 (2014).

12. Dustin, M.L. & Baldari, C.T. The Immune Synapse: Past, Present, and Future. *Methods Mol Biol* **1584**, 1-5 (2017).

13. Carpen, O., Virtanen, I., Lehto, V.P. & Saksela, E. Polarization of NK cell cytoskeleton upon conjugation with sensitive target cells. *J Immunol* **131**, 2695-2698 (1983).

14. Lagrue, K.*, et al.* The central role of the cytoskeleton in mechanisms and functions of the NK cell immune synapse. *Immunol Rev* **256**, 203-221 (2013).

15. Ben-Shmuel, A., Sabag, B., Biber, G. & Barda-Saad, M. The Role of the Cytoskeleton in Regulating the Natural Killer Cell Immune Response in Health and Disease: From Signaling Dynamics to Function. *Front Cell Dev Biol* **9**, 609532 (2021).

16. Bromley, S.K.*, et al.* The immunological synapse. *Annu Rev Immunol* **19**, 375-396 (2001).

17. Long, E.O., Kim, H.S., Liu, D., Peterson, M.E. & Rajagopalan, S. Controlling natural killer cell responses: integration of signals for activation and inhibition. *Annu Rev Immunol* **31**, 227-

555 258 (2013).

556

557 18. Topalian, S.L., Drake, C.G. & Pardoll, D.M. Immune checkpoint blockade: a common
558 denominator approach to cancer therapy. *Cancer Cell* **27**, 450-461 (2015).

559

560 19. Marin-Acevedo, J.A*., et al.* Next generation of immune checkpoint therapy in cancer: new
561 developments and challenges. *J Hematol Oncol* **11**, 39 (2018).

562

563 20. Qin, S*., et al.* Novel immune checkpoint targets: moving beyond PD-1 and CTLA-4. *Mol*
564 *Cancer* **18**, 155 (2019).

565

566 21. Norcross, M.A. A synaptic basis for T-lymphocyte activation. *Ann Immunol (Paris)* **135D**, 113-
567 134 (1984).

568

569 22. Sharma, K., Selzer, M.E. & Li, S. Scar-mediated inhibition and CSPG receptors in the CNS.
570 *Exp Neurol* **237**, 370-378 (2012).

571

572 23. Omotade, O.F., Pollitt, S.L. & Zheng, J.Q. Actin-based growth cone motility and guidance.
573 *Mol Cell Neurosci* **84**, 4-10 (2017).

574

575 24. Strittmatter, S.M. Modulation of axonal regeneration in neurodegenerative disease: focus on
576 Nogo. *J Mol Neurosci* **19**, 117-121 (2002).

577

578 25. Schwab, M.E. Functions of Nogo proteins and their receptors in the nervous system. *Nat*
579 *Rev Neurosci* **11**, 799-811 (2010).

580

581 26. Pernet, V. & Schwab, M.E. The role of Nogo-A in axonal plasticity, regrowth and repair. *Cell*
582 *Tissue Res* **349**, 97-104 (2012).

583

584 27. Niederost, B., Oertle, T., Fritsche, J., McKinney, R.A. & Bandtlow, C.E. Nogo-A and myelin-
585 associated glycoprotein mediate neurite growth inhibition by antagonistic regulation of
586 RhoA and Rac1. *J Neurosci* **22**, 10368-10376 (2002).

587

28. Schwab, M.E. & Strittmatter, S.M. Nogo limits neural plasticity and recovery from injury. *Curr Opin Neurobiol* **27**, 53-60 (2014).

29. Seiler, S., Di Santo, S. & Widmer, H.R. Non-canonical actions of Nogo-A and its receptors. *Biochem Pharmacol* **100**, 28-39 (2016).

30. Bakhuraysah, M.M.*, et al.* B-cells expressing NgR1 and NgR3 are localized to EAE-induced inflammatory infiltrates and are stimulated by BAFF. *Sci Rep* **11**, 2890 (2021).

31. GrandPre, T., Li, S. & Strittmatter, S.M. Nogo-66 receptor antagonist peptide promotes axonal regeneration. *Nature* **417**, 547-551 (2002).

32. Vesely, M.D., Kershaw, M.H., Schreiber, R.D. & Smyth, M.J. Natural innate and adaptive immunity to cancer. *Annu Rev Immunol* **29**, 235-271 (2011).

33. Cozar, B.*, et al.* Tumor-Infiltrating Natural Killer Cells. *Cancer Discov* **11**, 34-44 (2021).

34. Chiossone, L.*, et al.* Maturation of mouse NK cells is a 4-stage developmental program. *Blood* **113**, 5488-5496 (2009).

35. Mi, S.*, et al.* LINGO-1 is a component of the Nogo-66 receptor/p75 signaling complex. *Nat Neurosci* **7**, 221-228 (2004).

36. Park, J.B.*, et al.* A TNF receptor family member, TROY, is a coreceptor with Nogo receptor in mediating the inhibitory activity of myelin inhibitors. *Neuron* **45**, 345-351 (2005).

37. Filbin, M.T. Myelin-associated inhibitors of axonal regeneration in the adult mammalian CNS. *Nat Rev Neurosci* **4**, 703-713 (2003).

38. Wang, F. & Zhu, Y. The interaction of Nogo-66 receptor with Nogo-p4 inhibits the neuronal differentiation of neural stem cells. *Neuroscience* **151**, 74-81 (2008).

39. Maekawa, M.*, et al.* Signaling from Rho to the actin cytoskeleton through protein kinases

ROCK and LIM-kinase. *Science* **285**, 895-898 (1999).

40. Ridley, A.J. Rho GTPases and actin dynamics in membrane protrusions and vesicle trafficking. *Trends Cell Biol* **16**, 522-529 (2006).

41. Machacek, M.*, et al.* Coordination of Rho GTPase activities during cell protrusion. *Nature* **461**, 99-103 (2009).

42. Fritz, R.D.*, et al.* A versatile toolkit to produce sensitive FRET biosensors to visualize signaling in time and space. *Sci Signal* **6**, rs12 (2013).

43. Jung, T.Y.*, et al.* Nogo-A expression in oligodendroglial tumors. *Neuropathology* **31**, 11-19 (2011).

44. Giger, R.J.*, et al.* Mechanisms of CNS myelin inhibition: evidence for distinct and neuronal cell type specific receptor systems. *Restor Neurol Neurosci* **26**, 97-115 (2008).

45. Cao, Z.*, et al.* Receptors for myelin inhibitors: Structures and therapeutic opportunities. *Mol Cell Neurosci* **43**, 1-14 (2010).

46. Fry, E.J., Ho, C. & David, S. A role for Nogo receptor in macrophage clearance from injured peripheral nerve. *Neuron* **53**, 649-662 (2007).

47. Burshtyn, D.N., Shin, J., Stebbins, C. & Long, E.O. Adhesion to target cells is disrupted by the killer cell inhibitory receptor. *Curr Biol* **10**, 777-780 (2000).

48. Culley, F.J.*, et al.* Natural killer cell signal integration balances synapse symmetry and migration. *PLoS Biol* **7**, e1000159 (2009).

49. Lang, P.*, et al.* ADP-ribosylation of the ras-related, GTP-binding protein RhoA inhibits lymphocyte-mediated cytotoxicity. *J Biol Chem* **267**, 11677-11680 (1992).

50. Thauland, T.J., Hu, K.H., Bruce, M.A. & Butte, M.J. Cytoskeletal adaptivity regulates T cell

receptor signaling. *Sci Signal* **10** (2017).

51. Eibert, S.M.*, et al.* Cofilin peptide homologs interfere with immunological synapse formation and T cell activation. *Proc Natl Acad Sci U S A* **101**, 1957-1962 (2004).

52. Stebbins, C.C.*, et al.* Vav1 dephosphorylation by the tyrosine phosphatase SHP-1 as a mechanism for inhibition of cellular cytotoxicity. *Mol Cell Biol* **23**, 6291-6299 (2003).

53. Peterson, M.E. & Long, E.O. Inhibitory receptor signaling via tyrosine phosphorylation of the adaptor Crk. *Immunity* **29**, 578-588 (2008).

54. Newman, A.M.*, et al.* Robust enumeration of cell subsets from tissue expression profiles. *Nat Methods* **12**, 453-457 (2015).

55. Jin, H., Wan, Y.W. & Liu, Z. Comprehensive evaluation of RNA-seq quantification methods for linearity. *BMC Bioinformatics* **18**, 117 (2017).

## Acknowledgements

This work was supported by the National Research Council of Science & Technology (NST) grant by the Korea government (CAP-18-02-KRIBB).

## Author information

These authors contributed equally: Se-Chan Oh, Seong-Eun Kim.

## Affiliations

**Immunotherapy Research Center, Korea Research Institute of Bioscience and Biotechnology (KRIBB), Daejeon, Republic of Korea**

Se-Chan Oh, Seok-Min Kim, Soo Yun Lee, Sun-Young Lee and Tae-Don Kim

**Department of Functional Genomics, KRIBB School of Bioscience, Korea University of Science and Technology (UST), Daejeon, Republic of Korea**

Se-Chan Oh, Seok-Min Kim and Tae-Don Kim

**Department of Mechanical Engineering, Pohang University of Science and Technology (POSTECH), Pohang, Republic of Korea**

Seong-Eun Kim

**Department of Life Sciences, Korea University, Seoul, Republic of Korea**

Sun-Young Lee

**Genome Editing Research Center, Korea Research Institute of Bioscience and Biotechnology (KRIBB), Daejeon, Republic of Korea**

In Hwan Jang and In-Sun Chu

**Department of Bioinformatics, KRIBB School of Bioscience, Korea University of Science and Technology (UST), Daejeon, Republic of Korea**

In Hwan Jang and In-Sun Chu

**Department of Materials Science and Engineering, Research Institute of Advanced Materials (RIAM), Institute of Engineering Research, Seoul National University, Seoul 08826, Republic of Korea**

Junsang Doh

## Author contributions

T.-D.K. and J.D. conceived and designed the study. S.-C.O., S.-E.K. and I.H.J. aquired, analyzed and interpreted the data. J.D. and S.-E.K. designed the live image data. S.-M.K., S.Y.L and S.-Y.L. provided discussions and advice. I.H.J. and I.-S.C. designed and analyzed bioinformatic data. S.-C.O., S.-E.K., T.-D.K. and J.D. wrote, reviewed and revised the manuscript. T.-D.K. and J.D. supervised the study. T.-D.K. acquired funding.

## Corresponding authors

Correspondence to Junsang Doh or Tae-Don Kim

## Ethics declarations

## Competing interests

The authors declare no competing interests.

## Figure

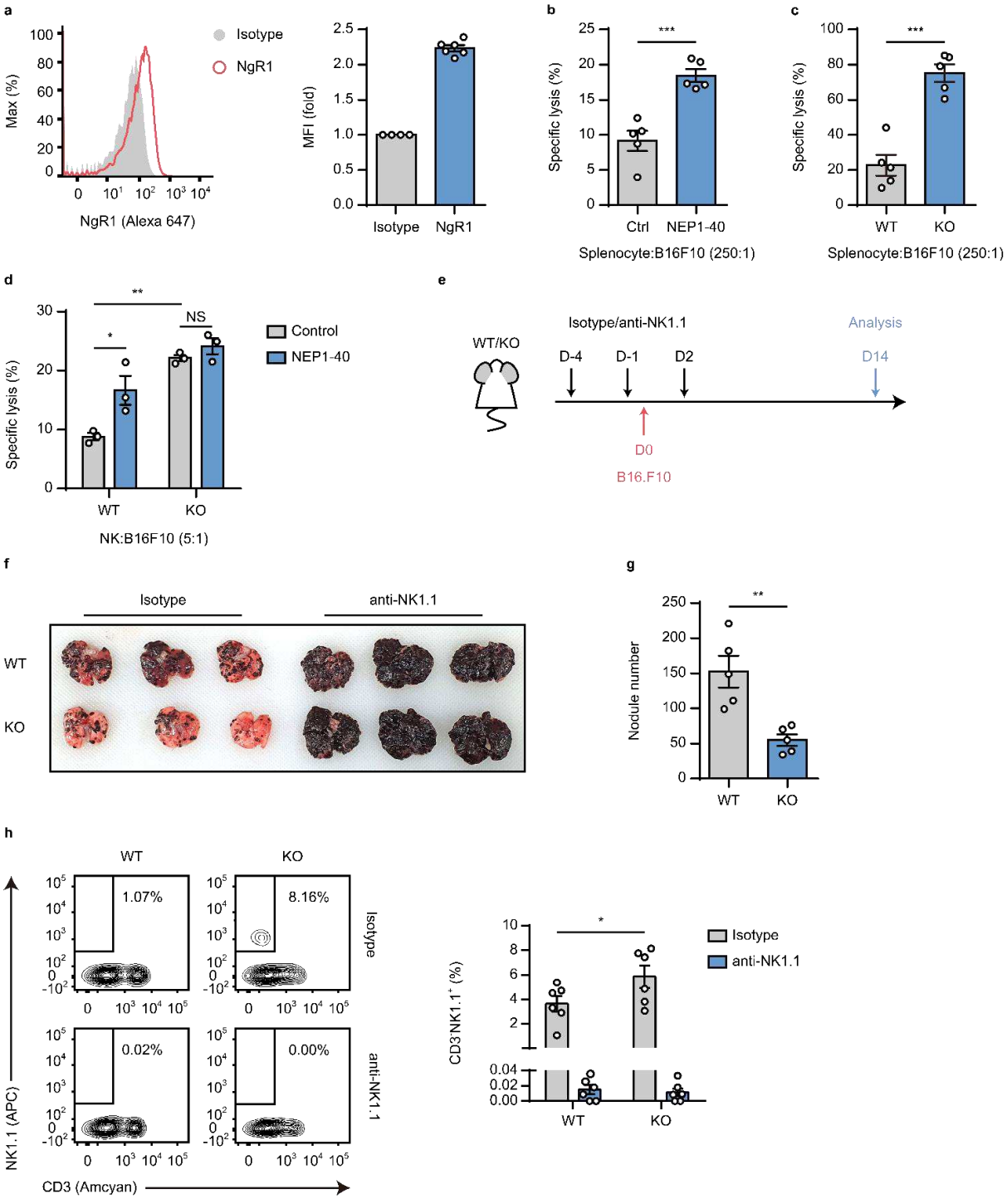

**Fig 1: NgR1 deficiency enhances a killing effects of NK cells in vitro and in vivo.**

**a**, Representative flow cytometric histograms and folds of MFI for NgR1 expression in splenic NK cells from WT mouse ($n$ = 4 Isotype, $n$ = 6 NgR1). **b**, Cytotoxicity analysis on B16F10 cells of splenocytes from WT mice with or without NEP1-40 treatment ($n$ = 6 each) (**b**), splenocytes from WT and KO mice ($n$ = 6 each) (**c**), and isolated splenic NK cells from WT and KO mice with or without NEP1-40 treatment ($n$ = 6 each) (**d**). **e**, Schematic of tumor and antibody administration of WT and KO mice. **f**, Representative lung images of WT and KO mice injected intravenously with isotype or NK1.1 antibody and B16F10 cells. **g**, Number of nodules formed in lungs of WT and KO mice ($n$ = 5 each). **h**, Representative flow cytometric plots and frequencies of intrapulmonary NK cells ($CD3^{-}NK1.1^{+}$) from WT and KO mice ($n$ = 6 each). In **a**-**d**,**g** and **h**, the data represent mean ± s.e.m. Statistical significance was determined by unpaired two-tailed Student`s t-test (**b**, **c** and **g**) or two-way ANOVA with Tukey`s multiple-comparisons test (**d** and **h**). $^{*}P < 0.05$, $^{**}P < 0.01$, $^{***}P < 0.001$.

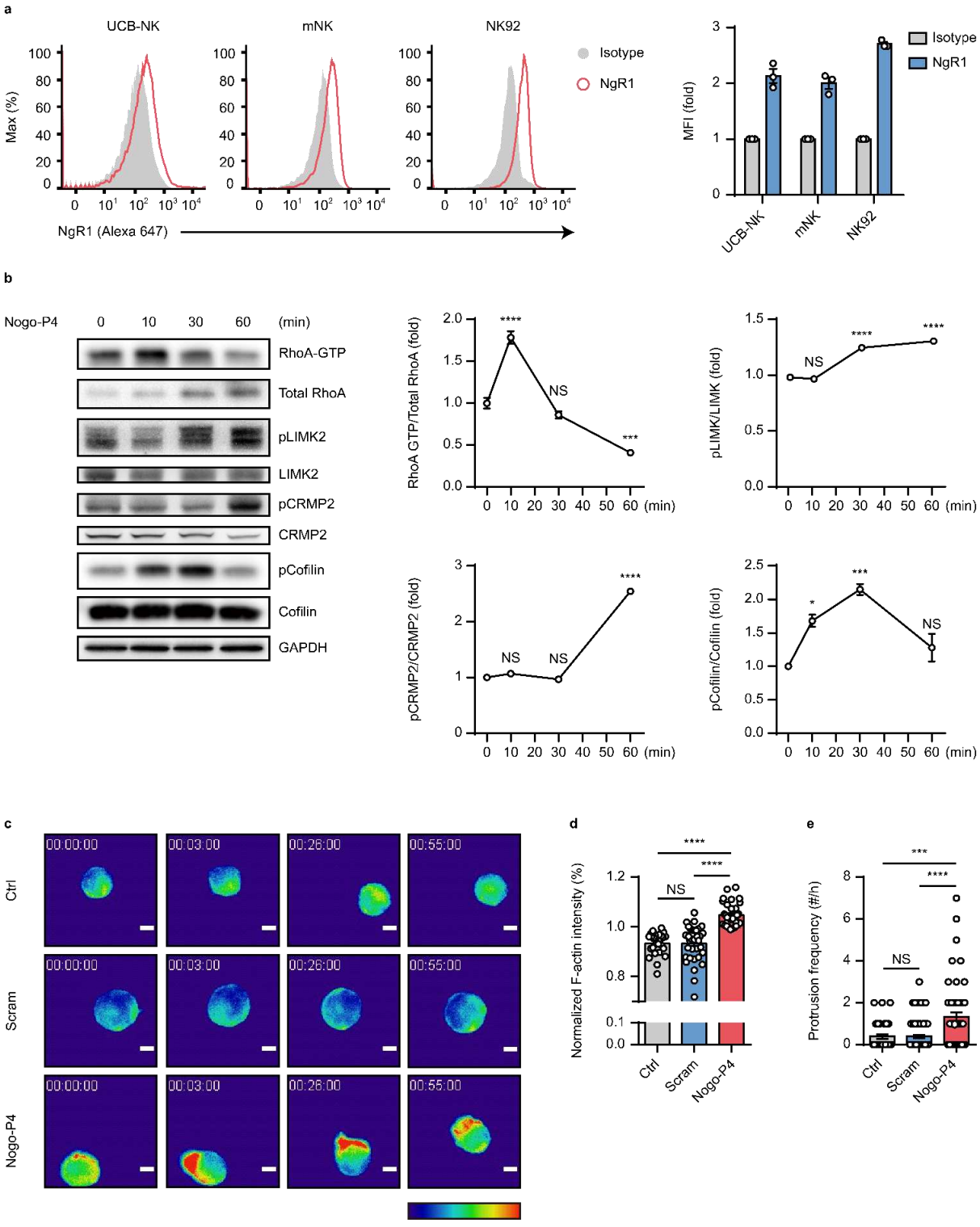


724

725 **Fig 2: NgR1 promotes F-actin polymerization in NK cells.**

726 **a**, Representative flow cytometric histograms and folds of MFI for NgR1 expression in
727 human UCB-NK, mNK and NK92 cells ($n$ = 3 each). **b**, Representative immunoblots and
728 quantification analysis of lysate from NK92 cells treated with Nogo-P4 during indicated time

(*n* = 3 each dots). **c**-**e**, Time lapse images for fluorescent intensity of NK92 cells expressing Lifeact-GFP with untreated (Ctrl), scrambled peptide (Scram) or Nogo-P4 treatment using video fluorescence microscopy. Scale bar, 5 μm. **d** and **e**, Single cell analysis for relative F-actin intensity (*n* = 26 Ctrl; *n* = 34 Scram; *n* = 33 Nogo-P4 ) (**d**) and protrusion frequency (*n* = 31 Ctrl; *n* = 65 Scram; *n* = 50 Nogo-P4) (**e**). In **a**, **b**, **d** and **e**, the data represent mean ± s.e.m. (**a**, **d** and **e**) or mean ± s.d. (**b**). Statistical significance was determined by one-way ANOVA with Tukey`s multiple-comparisons test (**b**,**d** and **e**). NS, not significant ($P > 0.05$); $^{**}P < 0.01$; $^{***}P < 0.001$; $^{****}P < 0.0001$.

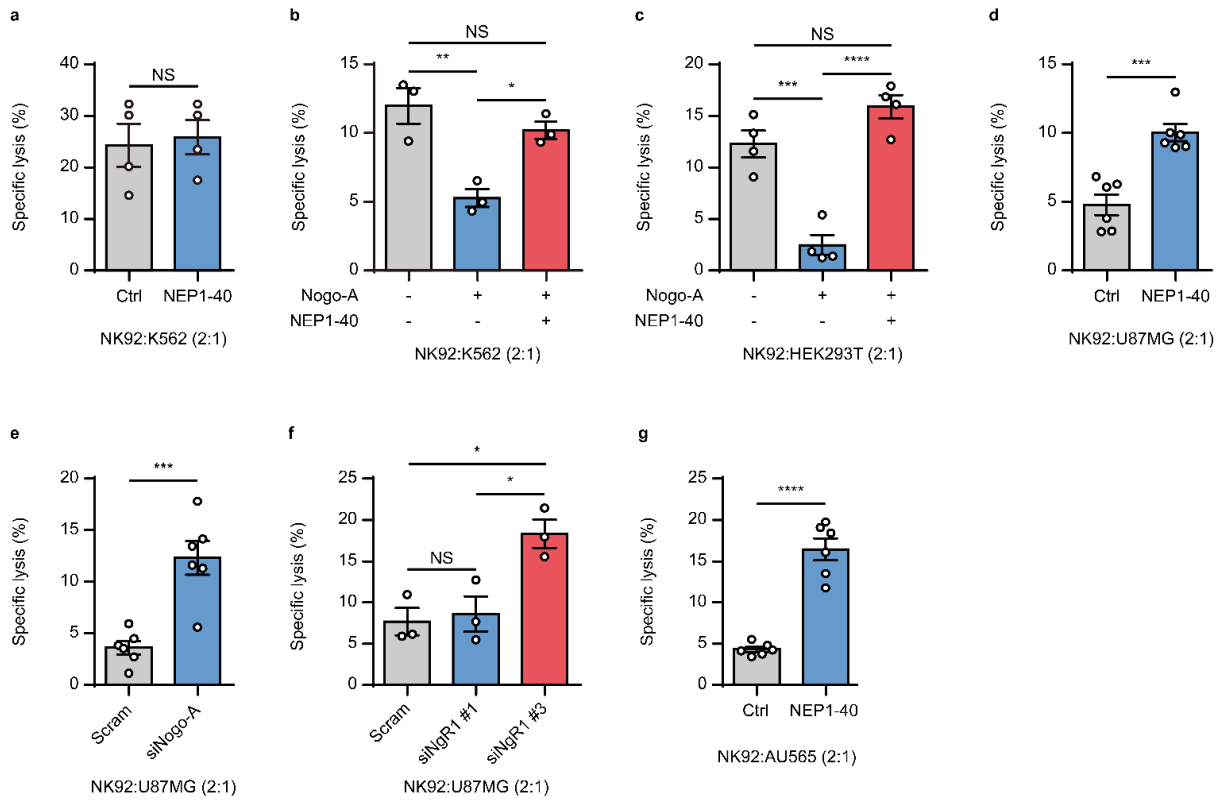


**Fig 3: NK cell-mediated cytotoxicity is suppressed by NogoA-NgR1-dependent manner.**

**a**-**g**, Cytotoxicity analysis of NK92 cells against to target cells. **a**-**d**, Cytotoxicity analysis of NK 92 cells to K562 cells (*n* = 4 each) (**a**), NogoA overexpressed K562 cells (*n* = 3 each) (**b**), NogoA overexpressed HEK293T cells (*n* = 4 each) (**c**), U87MG cells (*n* = 6) (**d**) with and without NEP1-40 treatment. **e**, Cytotoxicity analysis of NK92 cells against to U87MG cells suppressed Nogo-A expression (*n* = 6 each). **f**, Cytotoxicity analysis of NK92 cells with suppressed expression of NgR1 against to U87MG cells (*n* = 3 each). **g**, Cytotoxicity analysis

of NK 92 cells to AU565 cells with and without NEP1-40 treatment ($n$ = 6 each). In **a**-**g**, the data represent mean ± s.e.m. Statistical significance was determined by unpaired two-tailed Student`s $t$-test (**a**, **d**, **e** and **g**) or one-way ANOVA with Tukey`s multiple-comparisons test (**b**, **c**, **f**). NS, not significant ($P > 0.05$); *$P < 0.05$; **$P < 0.01$; ***$P < 0.001$; ****$P < 0.0001$.

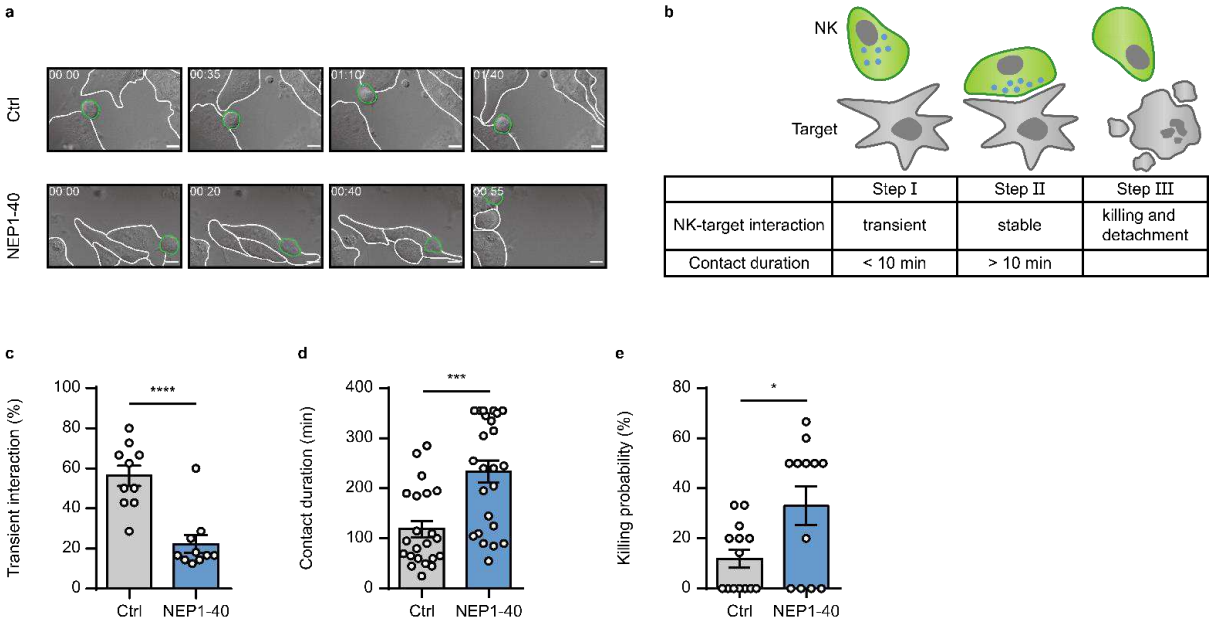


**Fig 4: NgR1 blockade positively regulates NK-to-target contact at early step.**

**a**, Representative time-lapse images of interaction between NK92 (yellow border line) and U87MG cells (white border line) with and without NEP1-40 treatment. Scale bar, 10 μm. **b**, Schematic of steps for NK-target interaction. **c**-**e**, Effects of NEP1-40 on NK92 transient interaction frequencies ($n$ = 10 each) (**c**), contact duration time ($n$ = 22 Ctrl, $n$ = 24 NEP1-40) (**d**) and killing probability (n = 14 Ctrl, n = 12 NEP1-40) (**e**). In **c**-**e**, the data represent mean ± s.e.m. Statistical significance was determined by unpaired two-tailed Student`s $t$-test (**c**-**e**). *$P < 0.05$, ***$P < 0.001$, ****$P < 0.0001$.

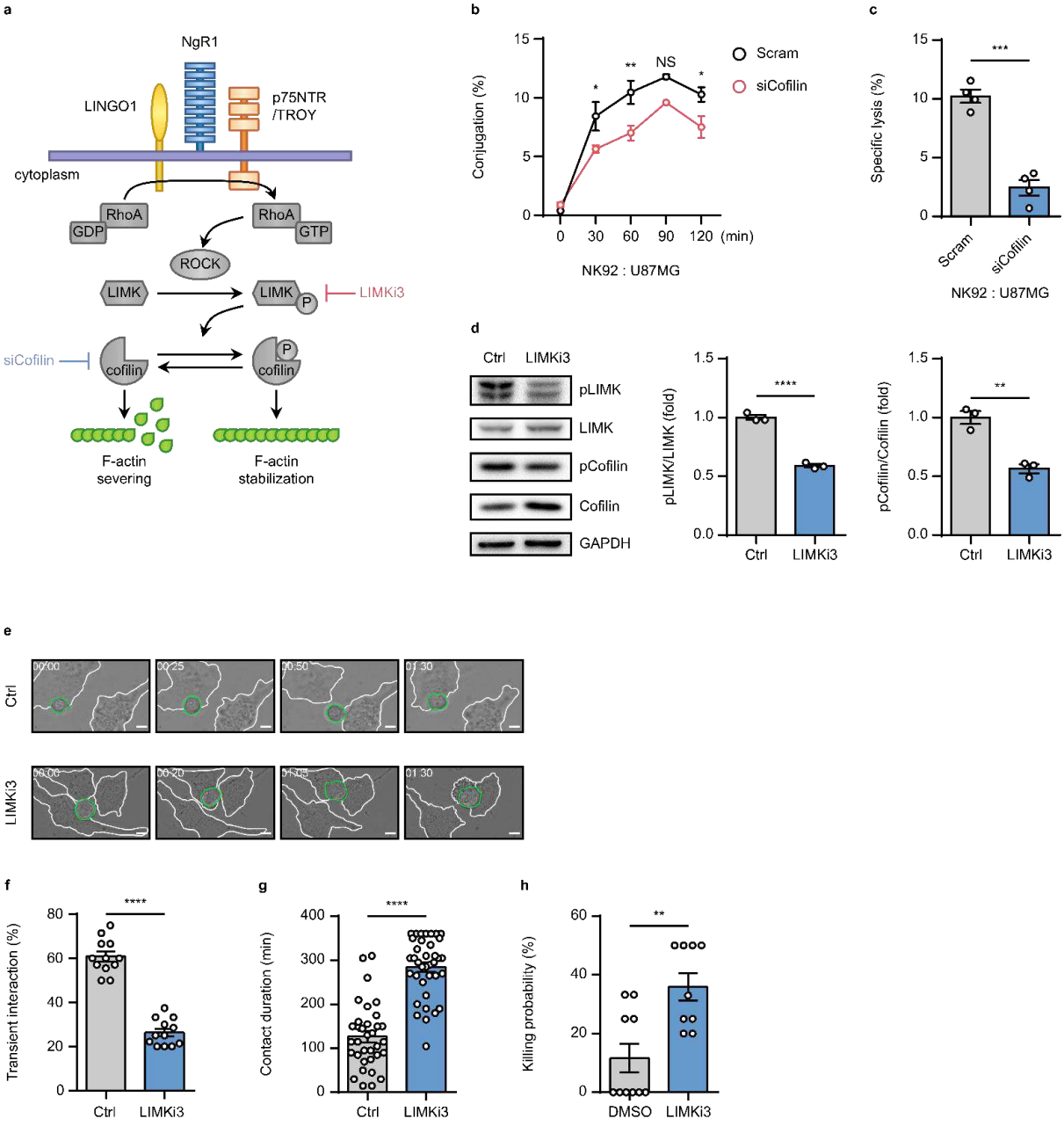


**Fig 5: NgR1 signals involved regulation of NK-target contact.**

**a**, Schematic of the downstream signals and inhibitors for NgR1. **b**, Conjugation frequencies between NK92 cells transfected with cofilin siRNA (siCofilin) and U87MG cells ($n$ = 3 each dots). **c**, Cytotoxicity analysis on U87MG cells of NK92 cells transfected with siCofilin ($n$ = 4 each). **d**, Representative immunoblots and quantification analysis of lysate from NK92 cells with and without LIMKi3 treatment incubated with U87MG cells. ($n$ = 3 each). **e**, Representative time-lapse images of interaction between NK92 (yellow border line) with and without LIMKi3 treatment and U87MG cells (white border line). Scale bar, 10 μm. **f**-**g**, Effects

of LIMKi3 on NK transient interaction frequencies ($n$ = 12 each) (**f**), contact duration time ($n$ = 34 Ctrl, $n$ = 37 LIMKi3) (**g**) and killing probability (n = 10 Ctrl, n = 9 LIMKi3) (**h**). In **b**-**d** and **f**-**h**, the data represent means ± s.e.m. (**b**, **c**, **f**, **g** and **h**) or mean ± s.d. (**d**) Statistical significance was determined by two-way ANOVA with Sidak`s multiple-comparisons test (**b**) or unpaired two-tailed Student`s $t$-test (**c**, **d** and **f**-**h**). $^{**}P < 0.01$, $^{***}P < 0.001$, $^{****}P < 0.0001$.

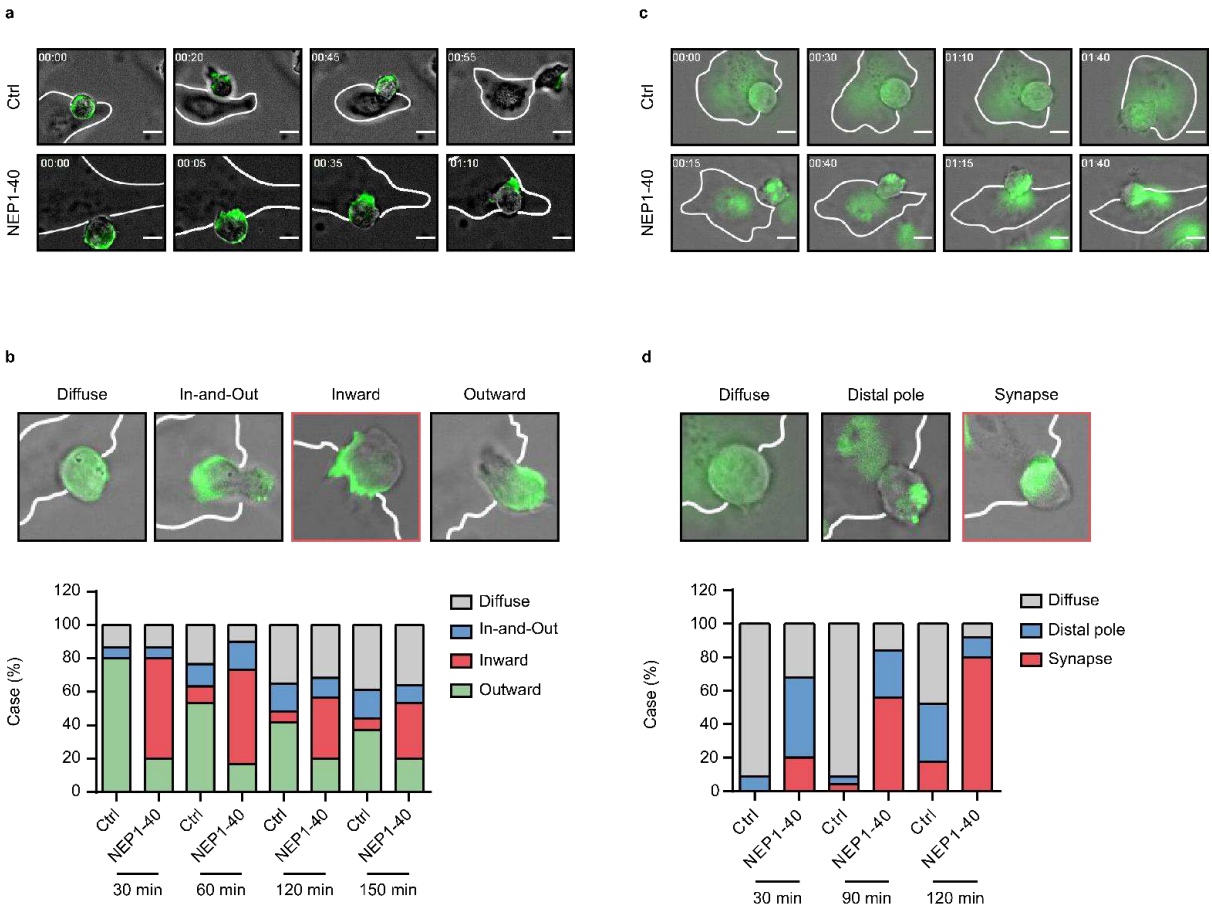


**Fig 6: IS is stably formed by NgR1 blockade.**

**a**, Representative time-lapse images during incubation of Lifeact-GFP-expressing NK92 cells and U87MG cells with untreated (Ctrl) and NEP1-40 treatment. Scale bar, 10 μm. **b**, Representative images of F-actin distribution cases (upper panel) and frequency analysis (bottom panel) in NK92 cells cultured with U87MG cells during indicated time with and without NEP1-40 treatment. **c**, Representative time-lapse images of lytic granules in NK92 cells incubated with U87MG cells under untreated (Ctrl) and NEP1-40 treatment. Scale bar, 10 μm. **d**, Representative images of lytic granule polarization cases (upper panel) and frequency analysis (bottom panel) in NK92 cells cultured with U87MG cells during indicated time.

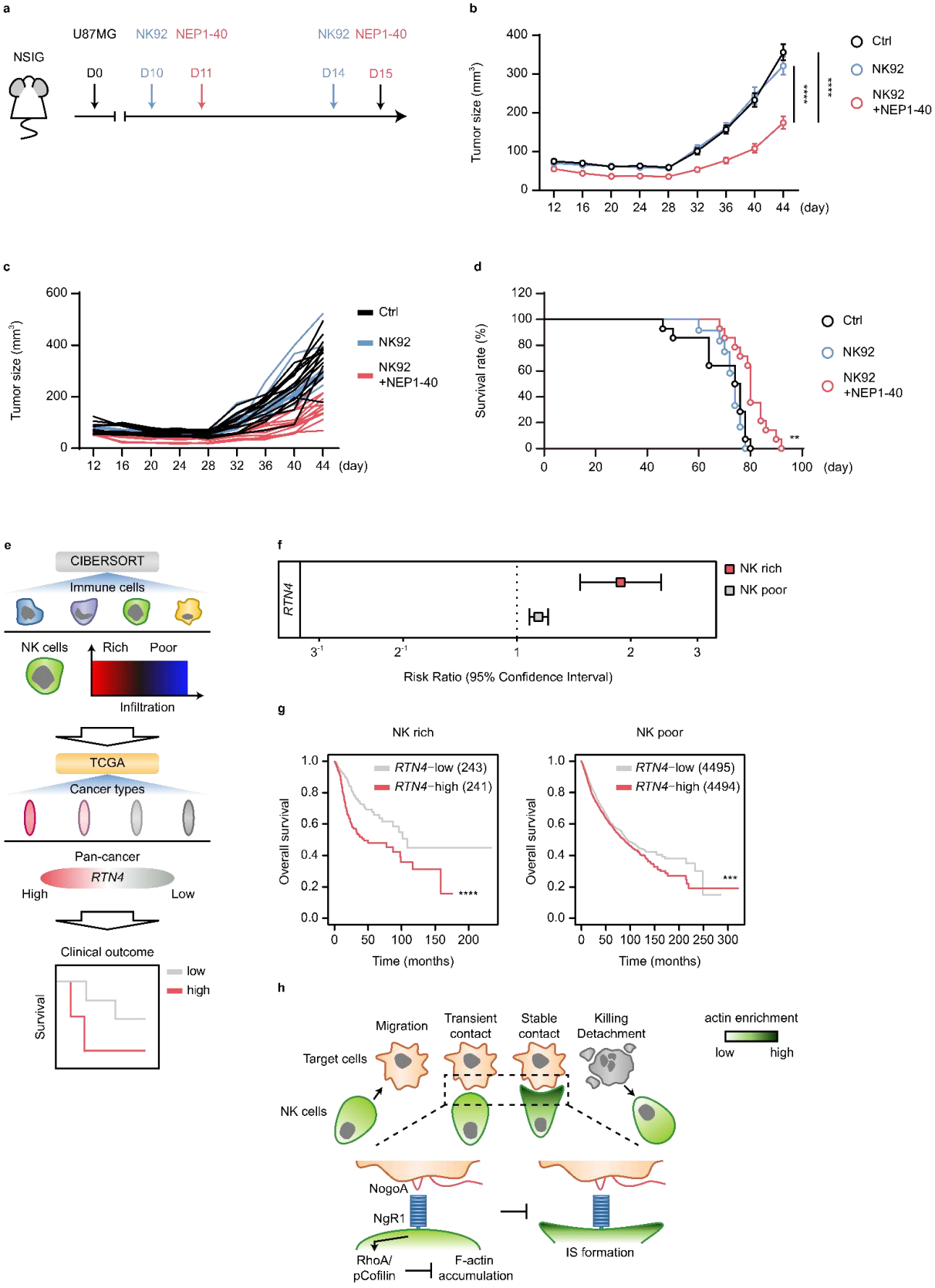


**Fig 7: NgR1 is a negative regulator for tumor control.**

**a**, Schematic of tumor, NK92 and peptide administration of NSIG mice. **b** and **c**, Average (**b**) and individual (**c**) tumor size of each conditions ($n$ = 14 Ctrl, $n$ = 11 NK92, $n$ = 14 NK92+NEP1-40) **d**, Survival rate of indicated conditions ($n$ = 11 Ctrl, $n$ = 12 NK92, $n$ = 14 NK92+NEP1-40) **e**, Diagram of the immune cell dependent survival analysis in large-scale cancer types profiled from TCGA. **f**, Cox hazard ratio of *RTN4* expression level stratified by the quantity of infiltrated NK cells at the top 20% in TCGA pan-cancer. **g**, Kaplan-Meir plot of *RTN4* expression level on top 20% NK-rich and bottom 80% NK-poor groups. **h**, Schematic cartoon for the role of NgR1 in NK cells. In **b**, **c** and **f**, the data represent mean ± s.e.m. Statistical significance was determined by two-way ANOVA with Sidak`s multiple-comparisons test (**b**), Gehan-Vreslow-Wilcoxon test (**c**) or log-rank test (**g**). $^{**}P < 0.01$, $^{***}P < 0.001$, $^{****}P < 0.0001$.

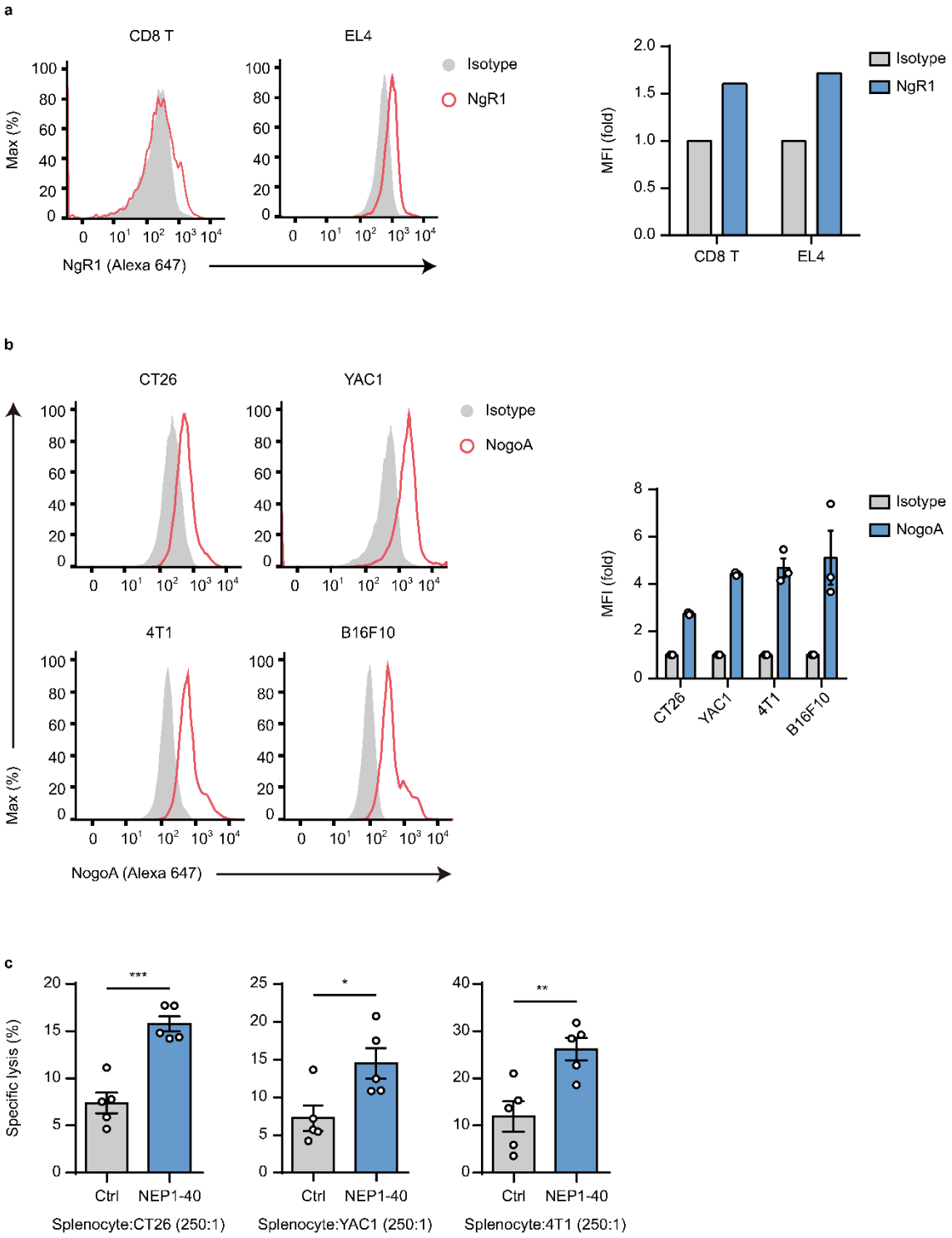


## Extended Data Fig 1:

**a**, Representative flow cytometric histograms and folds of MFI for NgR1 expression in splenic CD8 T cells from WT mouse and EL4 cell line ($n$ = 1 each). **b**, Representative flow cytometric histograms and folds of MFI for NogoA expression in CT26, YAC1, 4T1, and

B16F10 cell lines ($n$ = 3 each). **c**, Cytotoxicity analysis on CT26, YAC1, and 4T1 cells of splenocytes from WT mice with or without NEP1-40 treatment ($n$ = 6 each). In **b** and **c**, the data represent mean ± s.e.m. Statistical significance was determined by unpaired two-tailed Student`s $t$-test (**c**). $*P < 0.05$, $**P < 0.01$, $***P < 0.001$.

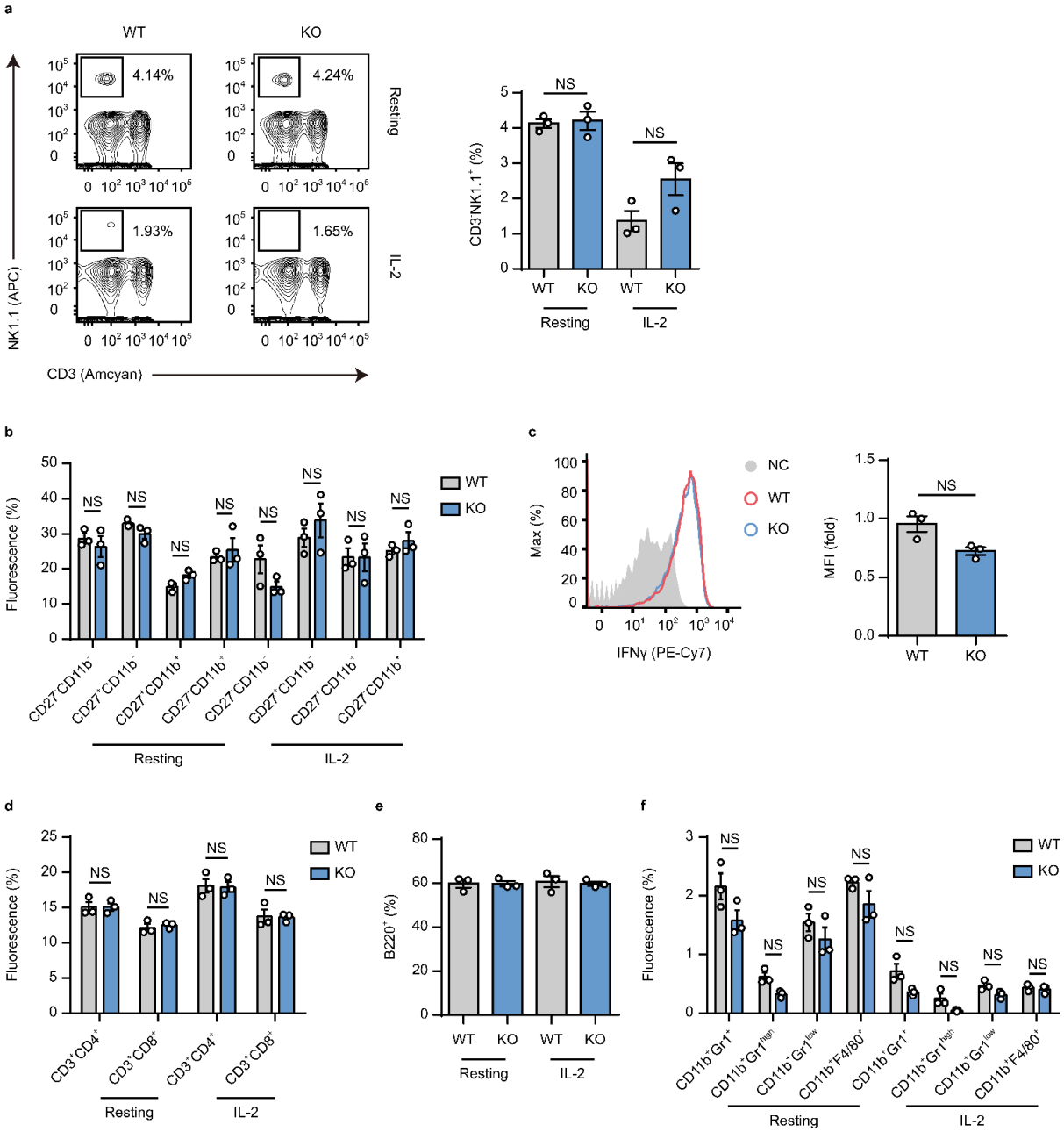


## Extended Data Fig 2:

**a**-**b**, Representative flow cytometric plots and frequencies of total NK cells ($CD3^-NK1.1^+$) and classified NK cells ($CD27^-CD11b^-$, $CD27^+CD11b^-$, $CD27^+CD11b^+$, $CD27^-CD11b^+$) with

or without IL-2 stimulation in WT and KO mice ($n = 3$ each). **c**, Representative flow cytometric histograms and folds of MFI for intracellular IFNγ expression of total NK cells in WT and KO mice ($n = 3$ each). **d-f**, Frequencies of resting or IL-2 stimulated CD4 T cells ($CD3^+CD4^+$) and CD8 T cells ($CD3^+CD8^+$) ($n = 3$ each) (**d**), B cells ($B220^+$) ($n = 3$ each) (**e**), and myeloid cells ($CD11b^+Gr1^+$), neutrophils ($CD11b^+Gr1^{high}$), monocytes ($CD11b^+Gr1^{low}$), and macrophages ($CD11b^+F4/80^{high}$) (**f**) in WT and KO mice. The data represent mean ± s.e.m. Statistical significance was determined by one-way ANOVA with Tukey`s multiple-comparisons test (**a** and **c**), two-way ANOVA with Tukey`s multiple-comparisons test (**b**, **d** and **f**) or unpaired two-tailed Student`s *t*-test (**c**). NS, not significant ($P > 0.05$).

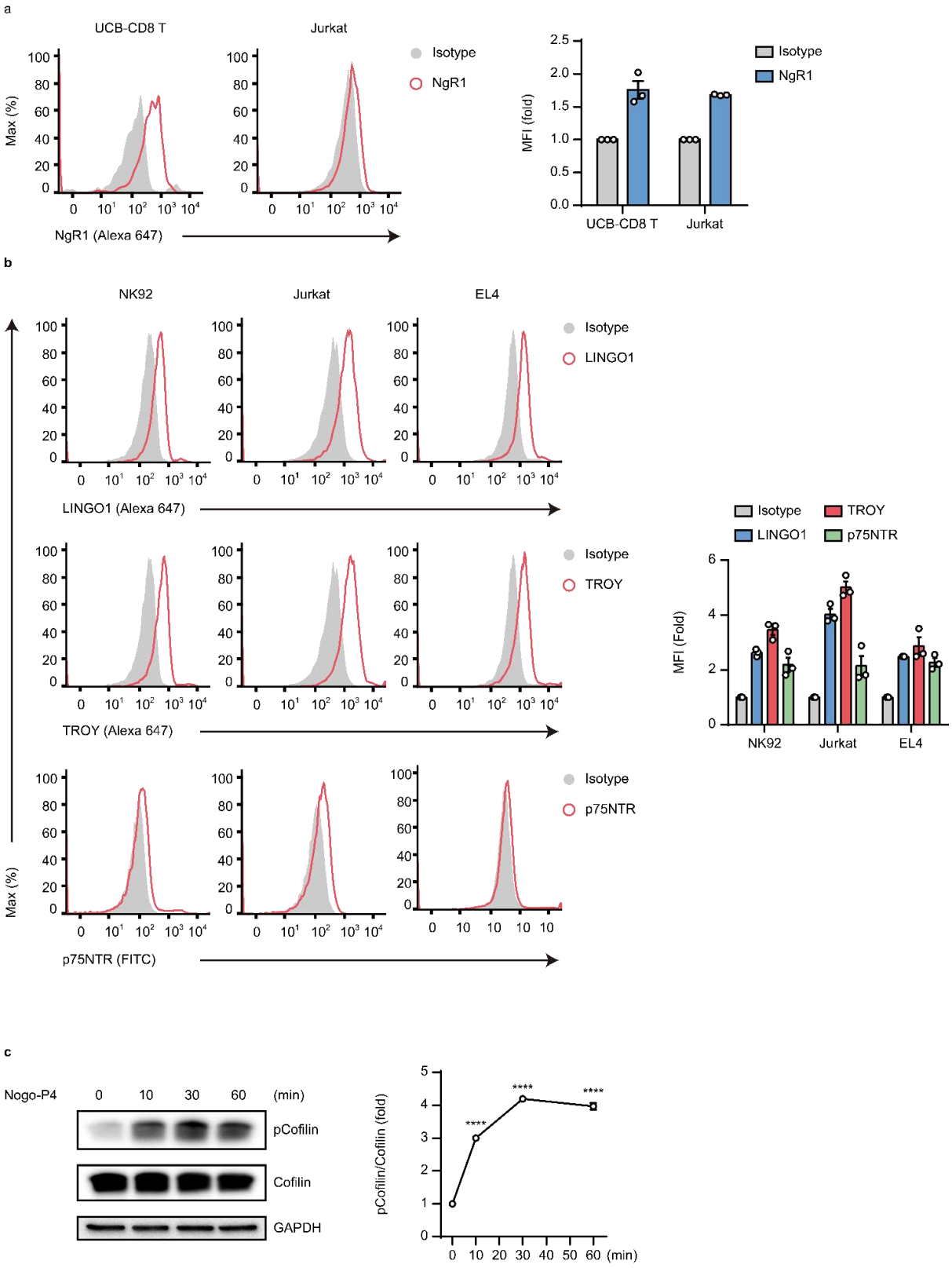


818

819 **Extended Data Fig 3:**

**a** and **b**, Representative flow cytometric histograms and folds of MFI for NgR1 expression in human UCB-CD8 T and Jurkat cell line ($n$ = 3 each) (**a**), and for LINGO1, TROY and p75NTR expression in NK92, Jurkat, EL4 cell lines ($n$ = 3 each) (**b**). **c**, Representative immunoblots and quantification analysis of lysate from human UCB-NK cells treated with Nogo-P4 during indicated time ($n$ = 3 each dots). The data represent mean ± s.e.m. (**a** and **b**) or mean ± s.d. (**c**). Statistical significance was determined by one-way ANOVA with Tukey`s multiple-comparisons test (**c**). ****$P$ < 0.0001.

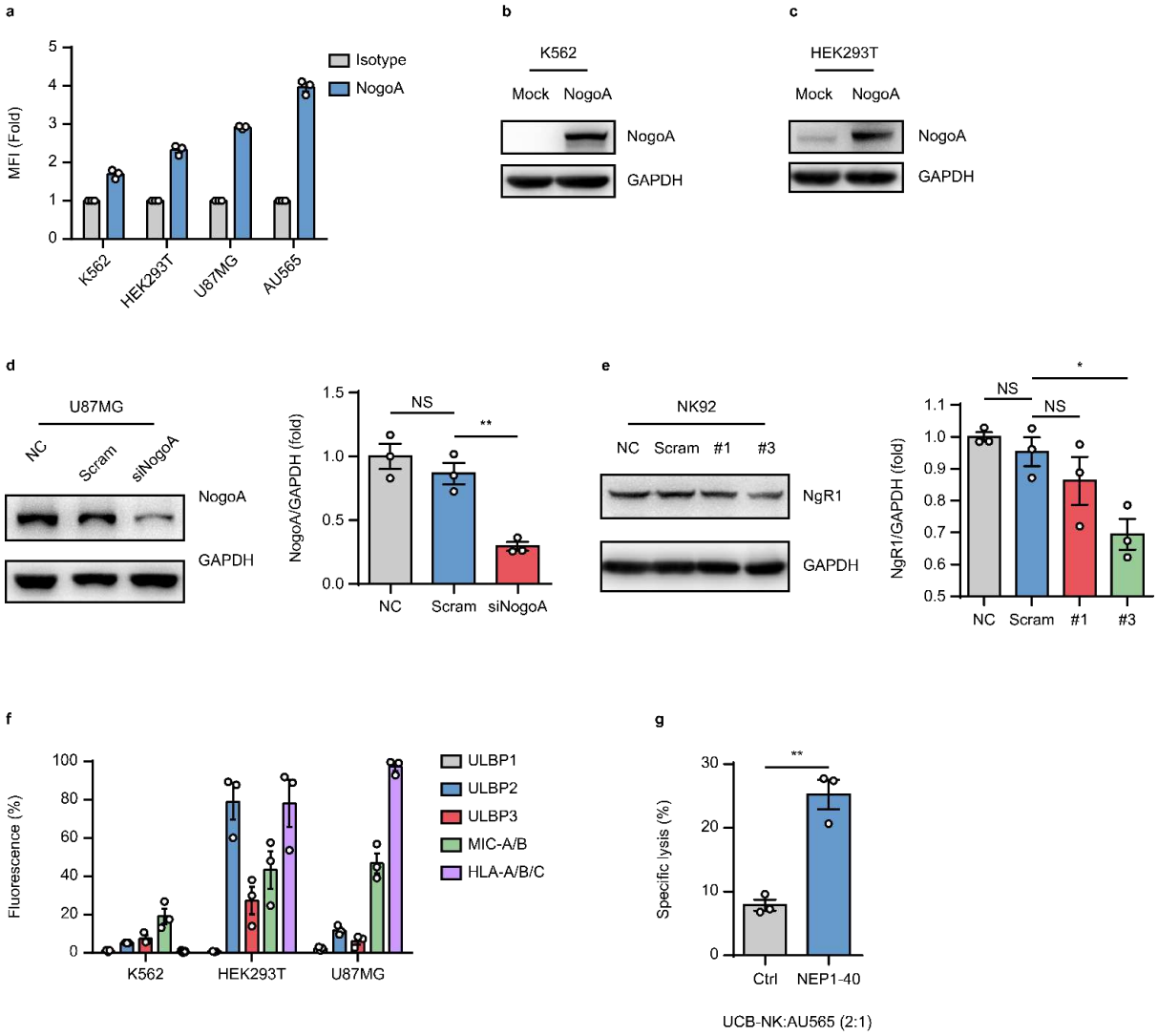


## Extended Data Fig 4:

**a**, Folds of MFI for NogoA expression in K562, HEK293T, U87MG and AU565 cell lines ($n$ = 3 each). **b** and **c**, Representative immunoblots of lysate from K562 or HEK293T cells overexpressed NogoA. **d**, Representative immunoblots and quantification analysis of lysate

from U87MG cells transfected scrambled siRNA (Scram) or NogoA siRNA (siNogoA) ($n$ = 3 each). **e**, Representative immunoblots and quantification analysis of lysate from NK92 cells transfected scrambled siRNA (Scram) or NgR1 siRNA #1 and #3 ($n$ = 3 each). **f**, Folds of MFI for ULBP1, ULBP2, ULBP3, MIC-A/B and HLA-A/B/C expression in K562, HEK293T, U87MG, AU565 cell lines ($n$ = 3 each). **g**, Cytotoxicity analysis of human UCB-NK cells to AU565 cells with or without NEP1-40 treatment ($n$ = 3 each). The data represent mean ± s.e.m. (**a**, **f** and **g**) or mean ± s.d. (**d** and **e**). Statistical significance was determined by one-way ANOVA with Tukey`s multiple-comparisons test (**d** and **e**) or unpaired two-tailed Student`s $t$-test (**g**). NS, not significant ($P > 0.05$); *$P < 0.05$; **$P < 0.01$.

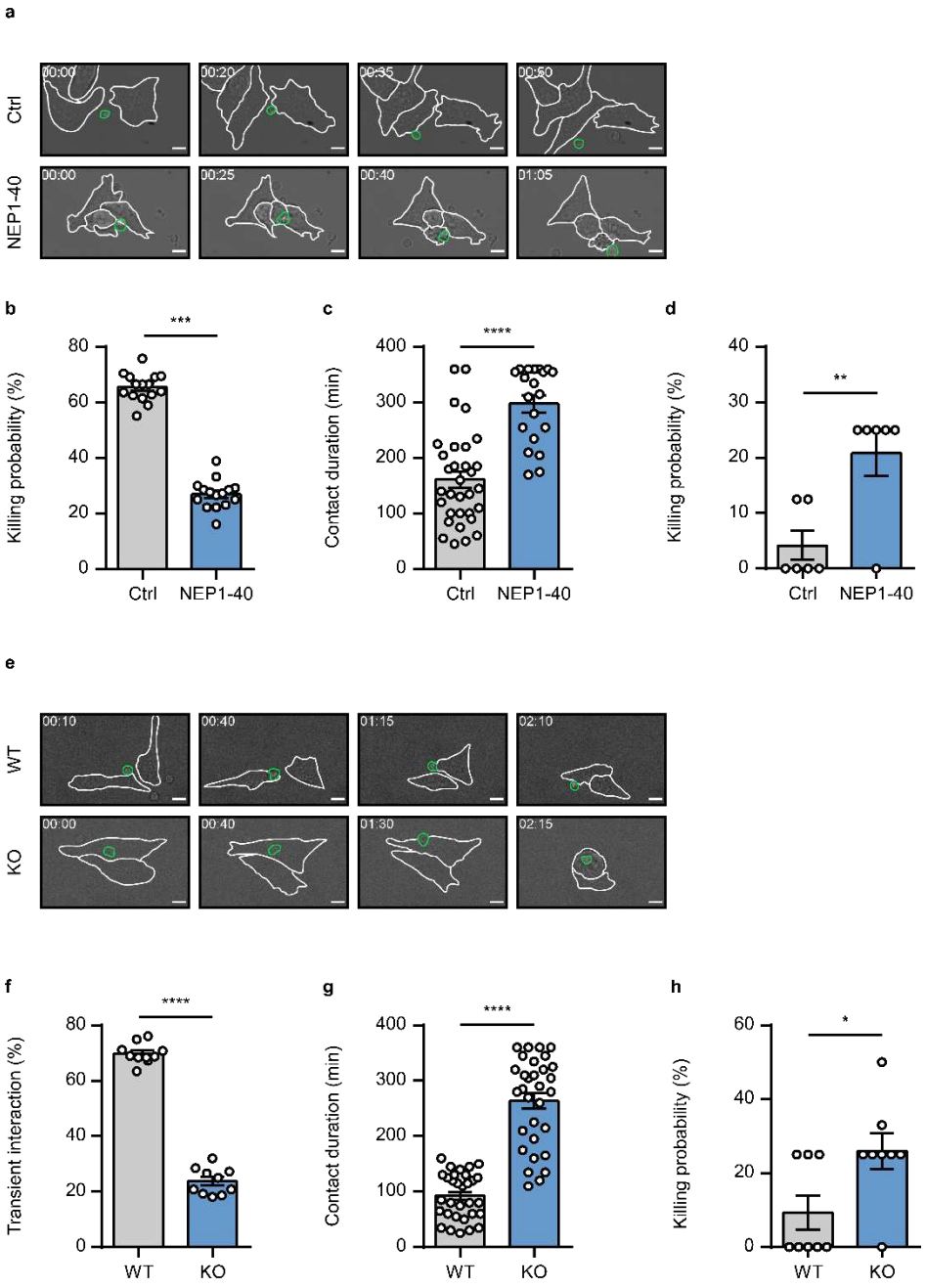


841

842 **Extended Data Fig 5:**

843 **a**, Representative time-lapse images of interaction between mouse NK cells (yellow border
844 line) and B16F10 cells (white border line) with and without NEP1-40. Scale bar, 10 μm. **b**-**d**,
845 Effects of NEP1-40 on NK transient interaction frequencies ($n$ = 15 each) (**b**), contact duration
846 time ($n$ = 32 Ctrl, $n$ = 20 NEP1-40) (**c**) and killing probability (n = 6 each) (**d**). **e**, Representative
847 time-lapse images of interaction between NK cells from WT and KO mice (yellow border line)
848 and B16F10 cells (white border line). Scale bar, 10 μm. **f**-**h**, Effects of KO on NK transient
849 interaction frequencies ($n$ = 10 each) (**f**), contact duration time ($n$ = 31 each) (**g**) and killing

probability (n = 8 each) (**h**). In **b**-**d** and **f**-**h**, the data represent mean ± s.e.m. Statistical significance was determined by unpaired two-tailed Student`s *t*-test (**b**-**d** and **f**-**h**). **P* < 0.05, ***P* < 0.01, ****P* < 0.001, *****P* < 0.0001.

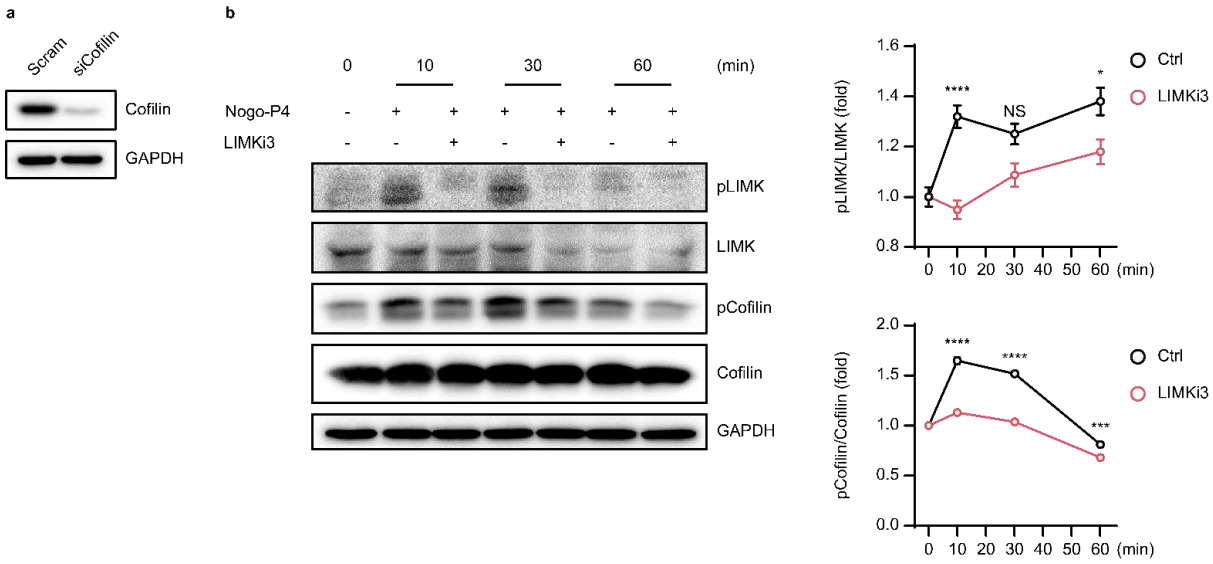


**Extended Data Fig 6:**

**a**, Representative immunoblots of lysate from NK92 cells with siCofilin transfection. **b**, Representative immunoblots and quantification analysis of lysate from NK92 cells with and without Nogo-P4 or LIMKi3 treatment during indicated time. (*n* = 3 each dots). The data represent mean ± s.d. Statistical significance was determined by two-way ANOVA with Sidak`s multiple-comparisons test (**b**). NS, not significant (*P* > 0.05); **P* < 0.05, ****P* < 0.001, *****P* < 0.0001.

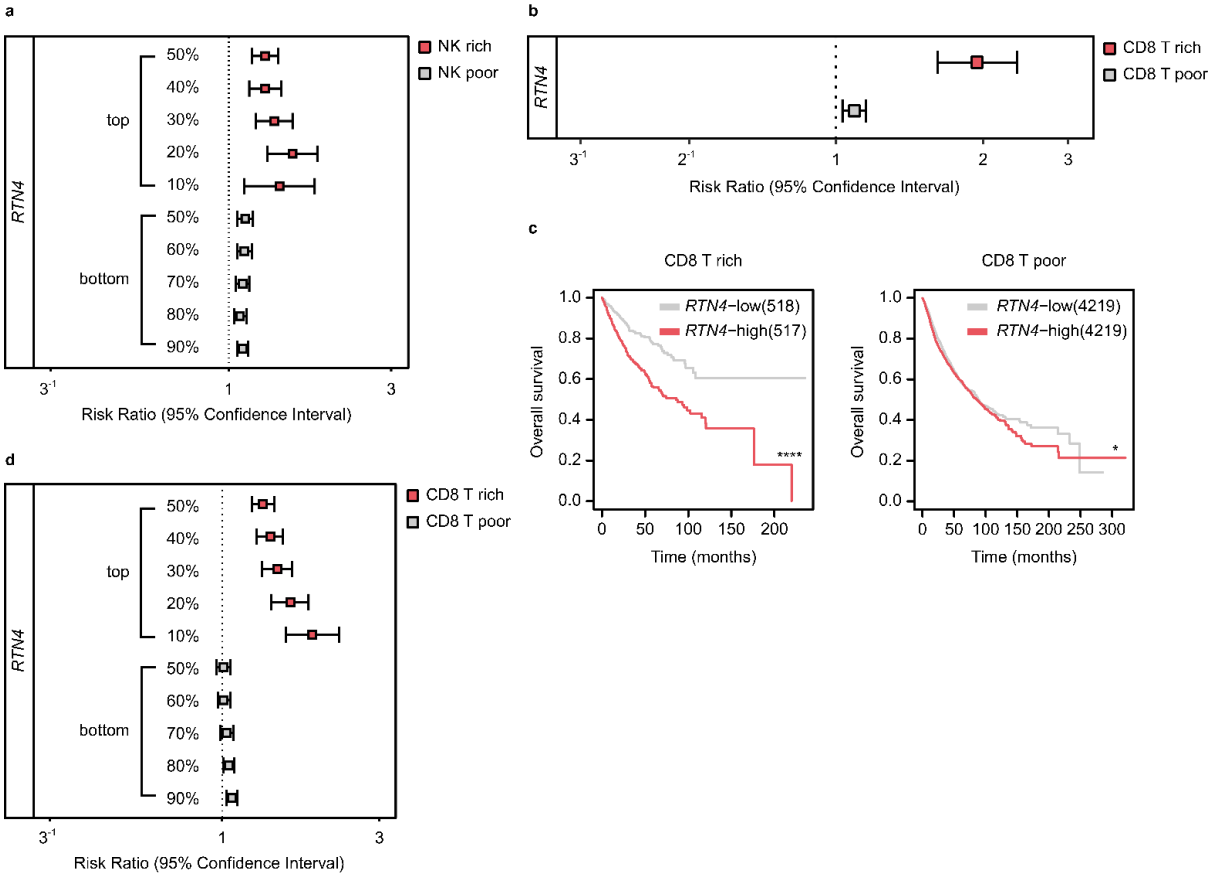


## Extended Data Fig 7:

**a**, Cox hazard ratio of *RTN4* expression level stratified by the quantity of infiltrated NK cells at the top 10% to 50% and the bottom 50% to 90% in TCGA pan-cancer. **b**, Cox hazard ratio of *RTN4* expression level stratified by the quantity of infiltrated CD8 T cells at the top 20% in TCGA pan-cancer. **c**, Kaplan-Meir plot of *RTN4* expression level on top 20% CD8 T-rich and bottom 80% CD8 T-poor groups. **d**, Cox hazard ratio of *RTN4* expression level stratified by the quantity of infiltrated CD8 T cells at the top 10% to 50% and the bottom 50% to 90% in TCGA pan-cancer. In **c**, the data represent mean ± s.e.m. Statistical significance was determined by log-rank test (**c**). **P* < 0.05, *****P* < 0.0001.

## Supplementary information

## Supplementary Video 1

Live imaging of NK92 cells expressing Lifeact-GFP incubated with untreated (Ctrl), scrambled peptide (Scram), or Nogo-P4 for indicated time using video microscopy.

**Supplementary Video 2**

Live imaging of co-culture of NK92 (green border line) and U87MG cells (white border line) with or without NEP1-40 treatment.

**Supplementary Video 3**

Live imaging of co-culture of NK cells (green border line) from WT mice and B16F10 cell line (white border line) with or without NEP1-40 treatment.

**Supplementary Video 4**

Live imaging of co-culture of NK cells (green border line) from WT or KO mice and B16F10 cell line (white border line).

**Supplementary Video 5**

Live imaging of co-culture of NK92 cells (green border line) pretreated with or without LIMKi3 and U87MG cells (white border line).

**Supplementary Video 6**

Live imaging of co-culture of NK92 cells expressing Lifeact-GFP (green) and U87MG cells (white border line) with or without NEP1-40 treatment.

**Supplementary Video 7**

Live imaging of co-culture of lysosensor (green) stained NK92 cells and U87MG cells (white border line) with or without NEP1-40 treatment.

| Cut-off | HR | lower | upper | *P*- value |
|---|---|---|---|---|
| NK top 50% | 1.28 | 1.17 | 1.4 | <0.0001 |
| NK top 40% | 1.28 | 1.15 | 1.43 | <0.0001 |
| NK top 30% | 1.36 | 1.2 | 1.54 | <0.0001 |
| NK top 20% | 1.54 | 1.3 | 1.82 | <0.0001 |
| NK top 10% | 1.41 | 1.11 | 1.79 | 0.005 |
| NK bottom 50% | 1.12 | 1.06 | 1.18 | <0.0001 |
| NK bottom 60% | 1.11 | 1.06 | 1.17 | <0.0001 |
| NK bottom 70% | 1.1 | 1.05 | 1.15 | <0.0001 |
| NK bottom 80% | 1.08 | 1.04 | 1.13 | 0.000 |
| NK bottom 90% | 1.1 | 1.06 | 1.14 | <0.0001 |

## Supplementary Table 1

Cox hazard ratio of *RTN4* expression level by quantity of infiltrated NK cells

| Cut-off | HR | lower | upper | *P*- value |
|---|---|---|---|---|
| CD8 T top 50% | 1.33 | 1.23 | 1.44 | <0.0001 |
| CD8 T top 40% | 1.4 | 1.27 | 1.53 | <0.0001 |
| CD8 T top 30% | 1.47 | 1.32 | 1.63 | <0.0001 |
| CD8 T top 20% | 1.61 | 1.41 | 1.83 | <0.0001 |
| CD8 T top 10% | 1.88 | 1.56 | 2.26 | <0.0001 |
| CD8 T bottom 50% | 1.01 | 0.96 | 1.06 | 0.658 |
| CD8 T bottom 60% | 1.01 | 0.97 | 1.06 | 0.546 |
| CD8 T bottom 70% | 1.03 | 0.99 | 1.08 | 0.131 |
| CD8 T bottom 80% | 1.05 | 1.01 | 1.09 | 0.02 |
| CD8 T bottom 90% | 1.07 | 1.03 | 1.11 | 0.001 |

## Supplementary Table 2

Cox hazard ratio of *RTN4* expression level by quantity of infiltrated CD8 T cells

# Supplementary Files

This is a list of supplementary files associated with this preprint. Click to download.

- 20220522SupplementaryTable.xlsx
- SupplementaryVideo.zip